Drug Annotation

Discovery of the 3-Imino-1,2,4-thiadiazinane 1,1-Dioxide Derivative Verubecestat (MK-8931)—A β-Site Amyloid Precursor Protein Cleaving Enzyme 1 Inhibitor for the Treatment of Alzheimer's Disease

Jack D. Scott,[*,†] Sarah W. Li,[†] Andrew P. J. Brunskill,[⊥] Xia Chen,[‡,■] Kathleen Cox,[§] Jared N. Cumming,[†] Mark Forman,[△] Eric J. Gilbert,[†] Robert A. Hodgson,[‡,□] Lynn A. Hyde,[‡] Qin Jiang,[▽] Ulrich Iserloh,[†,●] Irina Kazakevich,[∥] Reshma Kuvelkar,[‡] Hong Mei,[§] John Meredith,[¶] Jeffrey Misiaszek,[†,○] Peter Orth,[#] Lana M. Rossiter,[▽] Meagan Slater,[▽,▲] Julie Stone,[§] Corey O. Strickland,[#] Johannes H. Voigt,[#,◇] Ganfeng Wang,[§] Hongwu Wang,[#] Yusheng Wu,[†,◆] William J. Greenlee,[†,%] Eric M. Parker,[‡] Matthew E. Kennedy,[‡] and Andrew W. Stamford[*,†]

Departments of [†]Discovery Chemistry, [‡]Neuroscience, [§]Pharmacokinetics, Pharmacodynamics, and Drug Metabolism, [△]Translational Medicine, [#]Structural Chemistry, [⊥]Molecular and Materials Characterization, [∥]Pharmaceutical Sciences and Clinical Supply, and [¶]Toxicological Sciences, MRL, Merck & Co. Inc., 2015 Galloping Hill Road, Kenilworth, New Jersey 07033, United States

[▽]Albany Molecular Research Inc., 26 Corporate Circle, Albany, New York 12203, United States

Ⓢ Supporting Information

ABSTRACT: Verubecestat **3** (MK-8931), a diaryl amide-substituted 3-imino-1,2,4-thiadiazinane 1,1-dioxide derivative, is a high-affinity β-site amyloid precursor protein cleaving enzyme 1 (BACE1) inhibitor currently undergoing Phase 3 clinical evaluation for the treatment of mild to moderate and prodromal Alzheimer's disease. Although not selective over the closely related aspartyl protease BACE2, verubecestat has high selectivity for BACE1 over other key aspartyl proteases, notably cathepsin D, and profoundly lowers CSF and brain Aβ levels in rats and nonhuman primates and CSF Aβ levels in humans. In this annotation, we describe the discovery of **3**, including design, validation, and selected SAR around the novel iminothiadiazinane dioxide core as well as aspects of its preclinical and Phase 1 clinical characterization.
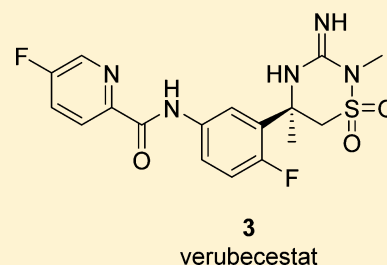

3
verubecestat

■ INTRODUCTION AND BIOLOGICAL RATIONALE

Alzheimer's disease (AD) is a devastating, progressive neurodegenerative disease that is associated with up to 80% of the estimated 47 million cases of dementia worldwide and is a leading cause of death in the United States.[1,2] As the elderly population increases, the worldwide incidence of dementia is expected to nearly triple to approximately 132 million by 2050, creating an unsustainable socioeconomic burden.[1] Currently available therapies, which include acetylcholinesterase inhibitors and the N-methyl-D-aspartate receptor antagonist memantine, produce modest and transient improvement in cognitive function but do not alter the progression of AD.[3] Treatments that delay or halt disease progression by targeting the underlying causes of AD would have lasting impacts on patient function and quality of life and would address an urgent unmet medical need.

Two histopathological hallmarks are invariably observed in the brains of AD patients, namely, extracellular amyloid plaques composed primarily of β-amyloid (Aβ) peptides and intraneuronal neurofibrillary tangles composed primarily of aggregates of abnormally phosphorylated tau protein. Aβ peptides are formed by two sequential cleavages of the amyloid precursor protein (APP), first by β-site amyloid precursor protein cleaving enzyme 1 (BACE1) followed by cleavage of the resulting C-terminal fragment C99 by γ-secretase. This cleavage sequence results in production of a family of Aβ peptides, of which Aβ40 is the most abundant isoform and Aβ42 is more highly prone to aggregate into neurotoxic, oligomeric species.[4] According to the amyloid hypothesis, aberrant production and/or accumulation of Aβ peptides, principally Aβ42, over a period of decades is causative of the underlying disease pathogenesis that ultimately leads to neuronal cell death.[4,5] In addition to the invariant presence of amyloid plaques in the brains of AD patients, the amyloid hypothesis is underpinned by several other lines of evidence. First, many distinct neurodegenerative diseases are associated with the invariant presence of abnormal protein aggregates analogous to amyloid plaques. Second, low levels of Aβ42 in the CSF are a reasonably good diagnostic/prognostic biomarker for AD. Finally, and most significantly, early onset autosomal dominant familial AD is associated with mutations in
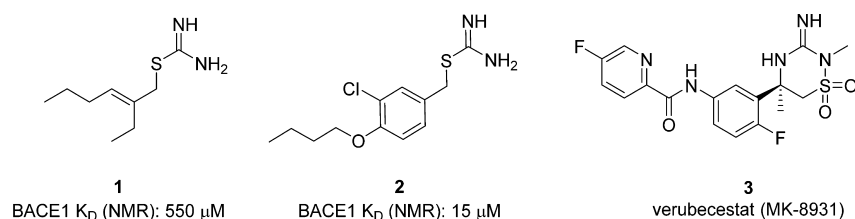
Figure 1. Structures of isothiourea NMR fragment screening hits and clinical compound **3**.
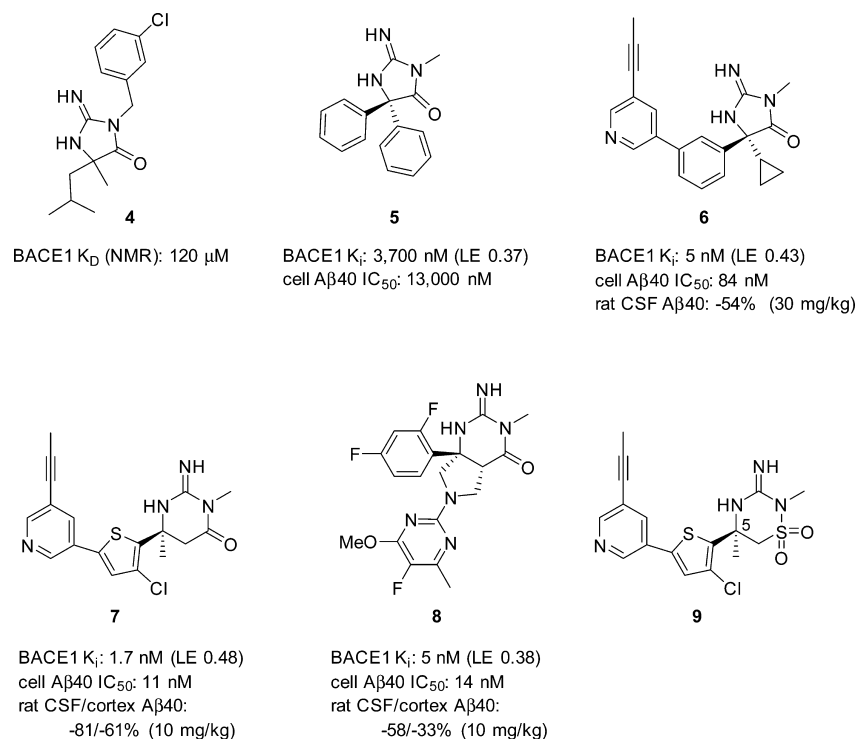

Figure 2. Iminoheterocyclic BACE1 inhibitors developed from isothiourea NMR fragment screening hits **1** and **2**.

APP and the presenilin proteins (which are components of the γ-secretase enzyme), and all of these mutations share the common phenotype of increasing total Aβ levels or the relative proportion of Aβ42.[6] Given this multifaceted evidence supporting the role of Aβ peptides in AD progression, substantial efforts have been invested in the development of amyloid-lowering therapies as a disease-modifying approach to AD treatment.[7] Prominent among these has been inhibition of BACE1 to reduce or prevent production of the Aβ peptides. This approach has been further supported by the recent finding that a rare mutation (A673T) near the BACE1 cleavage site in APP reduces Aβ peptide production and is associated with reduced risk of developing AD and improved cognitive function in the elderly.[8]

BACE1 is a membrane-bound aspartyl protease expressed primarily in the central nervous system (CNS), is the sole enzymatic activity responsible for the initial β-site APP cleavage, and is required for Aβ peptide production in vivo.[9] In the brain, BACE1 is expressed mainly in neurons and cleaves APP predominantly in the endosomal compartments where the acidic pH is near the optimum for its enzymatic activity (pH 5).[10] Since the characterization of BACE1 more than 15 years ago,[11] there have been intensive efforts to overcome the challenges of identifying small molecule inhibitors that can penetrate the CNS and inhibit the formation of centrally

derived Aβ peptides.[12] These efforts have been driven by evidence that BACE1 inhibition, in comparison with γ-secretase inhibition and antiamyloid immunotherapy, may be an inherently safer amyloid-lowering approach,[7] a notion that has been informed by an evolving understanding of BACE1 biology. In this regard, Bace1 knockout mice have been reported to have a number of subtle phenotypes, including reduction of central and peripheral nerve myelination, and several putative BACE1 substrates other than APP have recently been proposed.[10,13,14] However, many of these phenotypes and substrates remain to be independently confirmed, have little if any functional consequence, are not recapitulated by pharmacological inhibition of BACE, or may be mitigated through partial BACE1 inhibition.[8,10,13−15]

In this annotation, we describe the design and characterization of a novel iminothiadiazinane dioxide class of BACE1 inhibitors, originally derived from fragment screening hits **1** and **2** (Figure 1),[16] and key aspects of the extensive SAR explored around this core that culminated in the discovery of the highly optimized inhibitor verubecestat **3** (MK-8931, *N*-[3-[(5*R*)-3-amino-5,6-dihydro-2,5-dimethyl-1,1-dioxido-2*H*-1,2,4-thiadiazin-5-yl]-4-fluorophenyl]-5-fluoro-2-pyridinecarboxamide).[17] Compound **3** is currently in Phase 3 clinical trials with the potential to robustly test BACE1 inhibition as a disease-modifying treatment for AD.
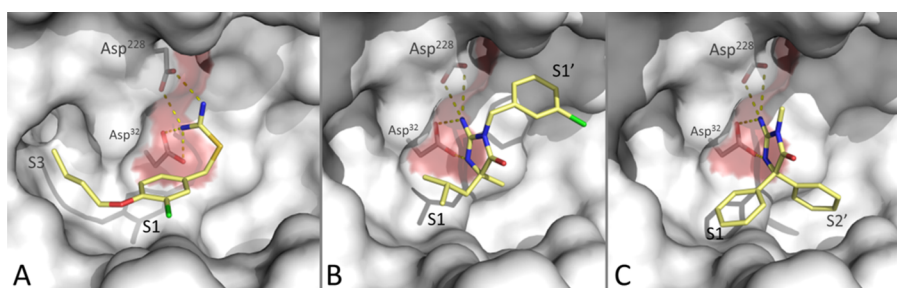
Figure 3. (A) BACE1 cocrystal with isothiourea hit **2**. (B) BACE1 cocrystal with designed iminohydantoin fragment **4**. (C) BACE1 cocrystal with lead iminohydantoin **5**. The flap residues of the enzyme have been removed for clarity. The surface of the two catalytic aspartic acids is colored salmon.

■ BACKGROUND

We have previously described the discovery of a series of iminoheterocyclic BACE1 inhibitors (Figure 2) originating from the isothiourea fragment screening hit **2** (Figure 1).[16,18] The isothiourea functionality of **2** engaged in hydrogen bond donor–acceptor interactions with the catalytic dyad of BACE1 (Asp[32] and Asp[228]), representing an aspartyl protease binding motif that was unprecedented at the time of its discovery (Figure 3A). Conceptually, the novel iminoheterocyclic class of aspartyl protease inhibitors was designed by replacing the isothiourea catalytic dyad binding motif with an iminoheterocyclic core embodied by iminohydantoin **4** (Figure 2). An X-ray cocrystal structure of BACE1 complexed with designed fragment **4** (Figure 3B) confirmed that the weakly basic amidine moiety engaged in a hydrogen bond donor–acceptor network with the catalytic dyad.[18] Through application of structure-based design with focus on balancing potency and lipophilicity, **4** was evolved into the highly ligand efficient diphenyl iminohydantoin lead compound **5** (Figure 3C).[18] Iminohydantoin **5** embodies the minimum BACE1 pharmacophore of a conformationally restricted benzyl amidine that projects the phenyl group into the hydrophobic S1 pocket.[19] Efficient occupancy of S3 and the S3 subpocket (S3[sp]) through structure-guided multiparameter optimization of this orally bioavailable, brain-penetrant lead resulted in the identification of iminohydantoin **6**,[20] which showed significant reduction of the pharmacodynamic biomarker, CSF Aβ40, after a single oral dose of 30 mg/kg to rats (Figure 2).

Subsequently, we disclosed a series of core-modified iminopyrimidinone BACE1 inhibitors with more potent pharmacodynamic activity exemplified by the high affinity and highly ligand efficient inhibitor **7**.[21] Following oral administration to rats, compound **7** exhibited robust, dose-dependent reductions of Aβ40 in CSF and cortex with ED$_{50}$ values of 4 and 6 mg/kg, respectively.[21] In an alternative display, an approach using structure-based design to build into a water-filled pocket of the enzyme near S2′ led to the discovery of the novel pyrrolidine-fused iminopyrimidinone analogue **8** that also showed robust CNS pharmacodynamic activity in rats with CSF and cortex Aβ40 oral ED$_{50}$ values of 5 and 13 mg/kg, respectively.[22] Although the discovery of the optimized inhibitors **6**−**8** represented significant advances, they did not meet criteria for long-term AD clinical trials, and further optimization efforts focused on addressing deficiencies in the profiles of these molecules.

■ COMPOUND DESIGN AND OPTIMIZATION

As a continuation of our efforts to discover BACE1 inhibitors with pharmacodynamic, pharmacokinetic, and safety profiles suitable for long-term clinical evaluation, we explored a series of iminothiadiazinane dioxides represented by **9** (Figure 2). We were attracted to the novel intellectual property space offered by the iminothiadiazinane dioxide motif as we anticipated increased competition in the iminoheterocyclic class of BACE1 inhibitors following the disclosure of cyclic acylguanidines in 2005−2006 by us and others.[23]

Modeling simulations of **9** suggested that replacement of the planar carbonyl group of **7** with the tetrahedral sulfonyl moiety would not significantly alter the conformational landscape; the required pseudoaxial orientation of the biaryl motif corresponding to the bound conformation of **9** was calculated to be close to the lowest energy conformation (within 0.5 kcal/mol of the energy minimum). In a model of **9** docked with the cocrystal structure of **7** and BACE1 (Figure 4A), the predicted binding modes of the iminothiadiazinane dioxide core and the S1−S3 biaryl motif of **9** were virtually superimposable with the crystal structure of **7**. In comparison to the iminopyrimidinone core, the slightly increased volume of the iminothiadiazinane ring and the steric demand of the sulfonyl group did not result in additional close contacts with the enzyme. The quaternary C5 methyl group of **9** projects toward the protein surface, and based on SAR developed in the iminopyrimidinone series[21] and the similar conformations of the iminopyrimidinone and iminothiadiazinane dioxide rings, groups larger than methyl at this position were unlikely to be tolerated due to steric clashes with the enzyme. With respect to calculated physicochemical properties, replacement of the carbonyl with sulfonyl was predicted to modestly increase PSA and decrease lipophilicity, remaining compatible with CNS penetration.

In the event, iminothiadiazinane dioxide **9** (K_i = 2.4 nM) was a potent BACE1 inhibitor with a K_i value similar to that of iminopyrimidinone **7** (Table 1). The X-ray crystal structure of **9** was almost superimposable with the bound structure of **7** (Figure 4B), consistent with the initial docking study. Although iminothiadiazinane dioxide **9** was equipotent to **7** in the purified enzyme assay, the compounds were differentiated on the basis of whole cell and in vivo activity and physical properties (Table 1). In comparison with **7**, iminothiadiazinane dioxide **9** was less potent in the cell-based assay with a more pronounced shift (23-fold) between the enzymatic K_i and cell IC$_{50}$ values despite its higher Caco-2 permeability. This may be a consequence of the reduced basicity of iminothiadiazinane dioxide **9** relative to its iminopyrimidinone counterpart **7** (Table 1) and is in agreement with literature reports and our
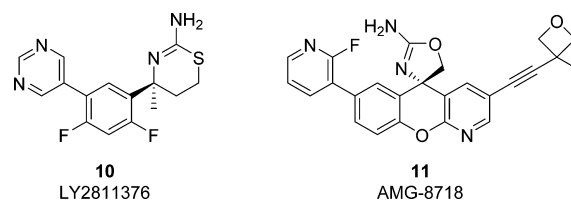
C
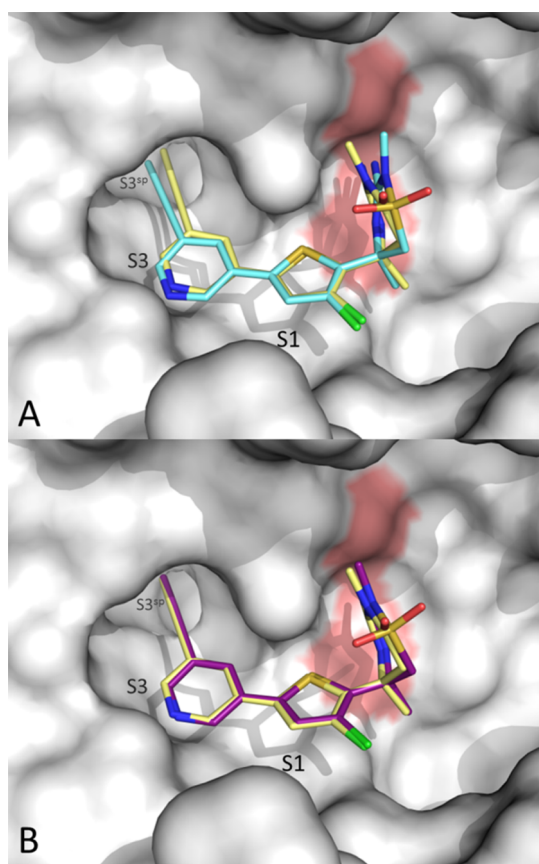
Figure 4. (A) Overlay of docked model of **9** (aqua) and the X-ray cocrystal structure of **7** (yellow) with BACE1. (B) X-ray cocrystal structures of **9** (purple; PDB: 5HTZ) and **7** (yellow) with BACE1.

Although the pharmacodynamic activities of analogues **7** and **9** were considered favorable for advancement, these compounds were not developed further. Metabolite profiling following oral administration of tritiated **9** to rats revealed biliary excretion of metabolites corresponding to direct glutathione addition and glutathione adducts derived from oxidative metabolism. Although not definitive, mass spectroscopy implicated the propynylpyridine moiety of **9** as the most likely site of glutathione addition. Additionally, the modest cathepsin D (CatD) selectivity of **7** and **9** (21- and 47-fold, respectively, based on enzyme K_i values) was considered to be inadequate and a major limitation to their progression. CatD, an aspartyl protease widely expressed in central and peripheral tissues, plays an essential role in lysosome function. Genetic deletion of CatD in mice results in neuronal lipopigment accumulation, neurodegeneration, blindness, and postnatal lethality. These phenotypes resemble neuronal ceroid lipofuscinosces, a group of rare human neurodegenerative disorders resulting from genetic disruption of lysosome function.[28]

Subsequent literature reports of the BACE1 inhibitors LY2811376 (**10**) and AMG-8718 (**11**) have substantiated toxicity concerns related to CatD inhibition (Figure 5).[29,30] In a

Figure 5. BACE1 inhibitors with potential CatD-mediated toxicity.

previous observations that related inhibitors such as **6** (pK_a 6.9) had decreased cellular potency relative to their K_i values as a function of their weaker basicities.[20,21,24,25] In an acute rat pharmacodynamic assay, **9** (10 mg/kg p.o.) afforded robust reductions of CSF and cortex $A\beta40$ levels. Although iminothiadiazinane dioxide **9** displayed weaker cellular potency than that of iminopyrimidinone **7**, it was significantly more potent than **7** in vivo based on comparison of unbound plasma concentrations that elicited similar central pharmacodynamic effects (Table 1). The greater in vivo potency of **9** is likely a consequence of improved permeability and enhanced CNS penetration imparted by the iminothiadiazinane dioxide core. In addition to favorable in vivo properties, iminothiadiazinane analogues had improved hydrolytic stability[27] (see Supporting Information) in comparison to the corresponding iminopyrimidinones, further validating the iminothiadiazinane dioxide core as a potentially druggable motif.

three month rat toxicology study of **10**, retinal photoreceptor degeneration, neuronal degeneration, and lipofuscinosis were observed, halting clinical evaluation of the compound.[29] Although the reported selectivity of **10** for BACE1 over CatD was 63-fold,[29] in our hands the selectivity is only 7-fold, supporting a role of CatD inhibition in the observed toxicity.[31] Additionally, BACE inhibitor **11** elicited retinal toxicity leading to thinning of the outer nuclear layer of the retina in a one month rat toxicity study.[30] Although the origin of the toxicity was not established, it was speculated that inhibition of other proteases including CatD may have contributed to the observed toxicity.

Given the concerns related to metabolism and CatD selectivity of **7** and **9**, we focused on modifications to the biaryl motif with the dual objectives of removal of the metabolically labile propynylpyridine and improvement of CatD selectivity. To this end, we had previously disclosed iminohydantoins **12** and **13** in which the two aryl groups

Table 1. Profile Comparsion between Iminopyrimidinone 7 and Iminothiadiazinane Dioxide 9

	BACE1 K_i [nM][a]	cell $A\beta40$ IC$_{50}$ [nM][b]	Caco-2 P_{app} [nm s^{-1}] (efflux ratio)	pK_a/ PSA[c]	CatD/ BACE1[d]	$A\beta40$ reduction CSF/ cortex[e] [%]	rat $C_{u,pl,3h,}$ [nM][f] (b/p)[g]	plasma f_u rat/ human [%]
7	1.7	11	153 (2.4)	7.5/69	21	−81/−61	33 (2.9)	3.6/1.6
9	2.4	55	278 (1.6)	6.6/86	47	−82/−53	8.0 (2.3)	1.6/0.7

[a]BACE1 K_i values were determined using purified human enzyme and are the mean of at least two determinations.[21] [b]IC$_{50}$ values were determined in HEK293 cells expressing human APP with the Swedish and London familial AD mutations.[18] [c]PSA was calculated as described in ref 26. [d]Ratio of K_i values. [e]Percent change relative to vehicle control 3 h after 10 mg/kg p.o. administration to rats. [f]Unbound plasma concentration 3 h after 10 mg/ kg p.o. administration to rats. [g]Ratio of total brain to total plasma compound concentrations.

binding in the enzyme S1 and S3 pockets are linked by a carboxamide (Figure 6).[32] Although the BACE1 affinity of
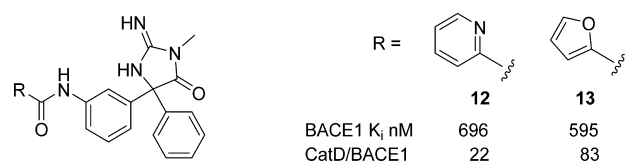

	12	**13**
BACE1 K_i nM	696	595
CatD/BACE1	22	83

Figure 6. Iminohydantoin S1−S3 amides.

these unoptimized analogues was relatively weak, they displayed some intrinsic selectivity over CatD. We were drawn to the unique binding features of the diaryl amide binding motif revealed by an X-ray cocrystal structure of (R)-**13** (Figure 7A) obtained from soaking the racemate whereby the
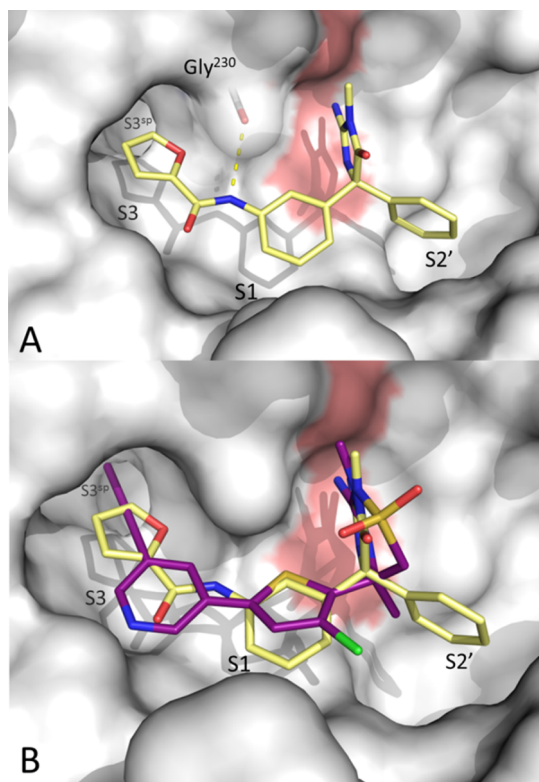

Figure 7. (A) Cocrystal structure of carboxamide (R)-**13** highlighting the hydrogen bond with BACE1 Gly[230] (PDB: 5HU0). (B) Overlay of the cocrystal structures of (R)-**13** (yellow) and **9** (purple) with BACE1.

phenyl and furanyl groups occupied the S1 and S3 pockets, respectively, and the amide N−H engaged in a hydrogen-bonding interaction with the carbonyl of Gly[230]. Additionally, the furanyl ring of (R)-**13** projected deeper into the S3 subpocket of BACE1 in comparison with the pyridyl ring of **9** (Figure 7B). On the basis of a comparison of the BACE1 and CatD crystal structures, their S3 subpockets differ in topology with the CatD S3 subpocket being slightly smaller than that of BACE1.[33] We postulated that differences in inhibitor binding in the S3 domains of the respective enzymes contributed to the modest selectivity of **13** over CatD. Thus, it was of interest to explore SAR targeting of this region as a means of gaining improved selectivity over CatD while maintaining high BACE1

affinity. A similar strategy has been employed in the hydroxyethylamine class of BACE inhibitors.[34]

Furthermore, in the course of our SAR investigations, we had observed that BACE1 affinity could be highly dependent on the iminoheterocyclic core for a given S1−S3 binding motif.[20] For example, in the iminohydantoin series, regioisomeric analogues **14** and **15** that bear an S1-binding thienyl group and an optimized cyclopropyl substituent,[20] were less potent than the corresponding S1 phenyl analogue **16** (Figure 8). The same
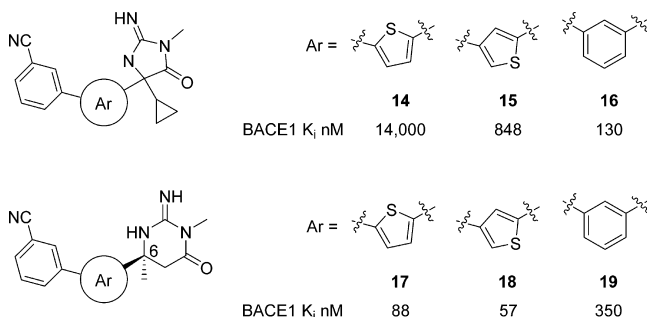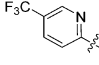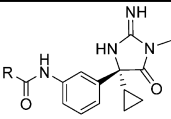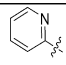

	14	**15**	**16**
BACE1 K_i nM	14,000	848	130

	17	**18**	**19**
BACE1 K_i nM	88	57	350
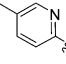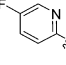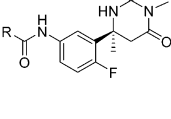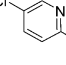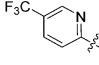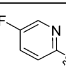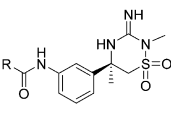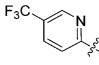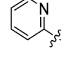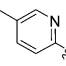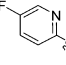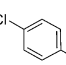
Figure 8. Iminohydantoin and iminopyrimidinone biaryl analogues.

rank order of affinity was observed for analogues of **14**−**16** in which the cyclopropyl group was replaced by methyl (not shown). Conversely, in the iminopyrimidinone biaryl series bearing a methyl group as the optimal quaternary C6 substituent, the thienyl analogues **17** and **18** were more potent than phenyl analogue **19**.[21] Most striking was the significant difference in K_i between the 2,5-thienyl analogues **14** and **17**. Accordingly, we prepared a series of iminohydantoin, iminopyrimidinone, and iminothiadiazinane dioxide derivatives bearing a diaryl amide motif to ascertain their BACE1 affinity and selectivity profiles.

Iminopyrimidinone **21** (Table 2) bearing a picolinamide substituent was an order of magnitude more potent than similarly substituted iminohydantoin **12** (Figure 6). We were gratified to find that novel iminothiadiazinane dioxide diaryl amide **27** also possessed high BACE1 affinity and was approximately 6-fold more potent than optimized iminohydantoin **20** bearing the matched diaryl amide motif. Strikingly, selectivity of the diaryl amides **21** and **27** for BACE1 inhibition relative to CatD was exceedingly high.

In the iminopyrimidinone series, introduction of a substituent at the pyridyl 5-position resulted in increased BACE1 affinity compared to that of **21** that lacks substitution at this position with the methyl, fluoro, chloro, and trifluoromethyl analogues (**22**−**25**) displaying single-digit to subnanomolar K_i values while maintaining high selectivity over CatD. Cell IC$_{50}$ values for these analogues were virtually unshifted relative to their K_i values. Introduction of the picolinamide scaffold also resulted in a significantly higher unbound plasma fraction compared to those of the biaryl analogues **7** and **9** with rat values in t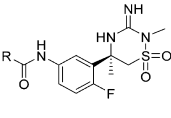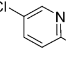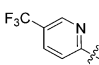he range of 15−40%. However, in comparison with **7** and **9**, picolinamide iminopyrimidinone analogues **23**−**25** displayed relatively modest reductions of CSF and cortex Aβ40 in the rat pharmacodynamic assay 3 h after oral administration (10 mg/kg) despite achieving similar unbound plasma concentrations. The more modest pharmacodynamic activities of iminopyrimidinones **23**−**25** compared to those of **7** and **9** is consistent with their significantly lower P_{app} values and higher

Table 2. N-Phenyl Carboxamide Analogues

Compound	R	core	BACE1 K_i [nM][a]	Cell IC$_{50}$ [nM][b]	CatD/ BACE1[c]	Caco-2 P_{app} [nm.s^{-1}] (ER)	Rat Aβ40 CSF/cortex [%][d]	Rat hepCl [μL/min/10^6 cells]	$C_{u,plasma}$ nM[e] (b/p)[f]
20			30	162	234	-	-	-	-
21			15	26	>1,000	25 (8.5)	-42/-26	23	38 (0.28)
22			4.2	3.0	>1,000	<1 (>23)	-4/-	35	2 (0.67)
23			4.0	4.6	>10,000	22 (11)	-53/-11	2.6	22 (0.38)
24			0.8	2.0	>10,000	<1 (>16)	-63/-19	8	30 (0.34)
25			3.8	7.0	>10,000	17 (11)	-61/0	4	43 (0.45)
26			10	5.8	>1,000	92 (2.3)	-35/	-	29 (0.52)
27			5.1	3.4	>10,000	72 (3.8)	-8/-	-	23 (0.81)
28			7.1	7.5	>1,000	74 (3.9)	-14/-	14	16 (0.49)
29			3	2	>10,000	151 (2.1)	-17/-	44	0.5 (-)
3 verubecestat			2.2	2.1	>10,000	128 (2.4)	-85/-53	3.1	36 (0.57)
30			0.9	1.0	>10,000	118 (3.1)	-93/-51	13	17 (0.89)
31			1.1	0.7	>10,000	89 (2.9)	-75/-31	11	25 (0.60)
32			13	15	>1,000	14 (16)	+18	6	9 (0.39)

[a]BACE1 K_i values were determined using purified human enzyme and are the mean of at least two determinations.[21] [b]IC$_{50}$ values were determined in HEK293 cells expressing human APP with the Swedish and London familial AD mutations.[18] [c]Ratio of mean K_i values. [d]Change in Aβ40 versus vehicle control 3 h after oral administration (10 mg/kg) of compound to rats. [e]Unbound plasma concentration of compound 3 h after oral administration to rats. [f]Ratio of total brain to total plasma compound concentrations.

Caco-2 efflux ratios, suggesting that reduced permeability and Pgp-mediated efflux restricts their brain penetration (vide infra). Methylpyridine 22 showed low plasma levels in the pharmacodynamic screen, likely as a consequence of its susceptibility to efflux and/or oxidative metabolism; the latter is consistent with the high rat hepatocyte clearance of 22 (35 μL min^{-1} [10^6 cells]$^{-1}$) compared to that of analogues 23−25 (≤8 μL min^{-1} [10^6 cells]$^{-1}$) that lack the pyridyl methyl group.

Similar SAR trends were observed for the novel iminothia-diazinane dioxide carboxamide analogues 3 and 28−31 with respect to BACE1 affinity, CatD selectivity, cell-based potency, and unbound plasma fraction. Comparison of the 6-fluorophenyl analogues 3 and 31 with the corresponding desfluoro analogues 26 and 27 demonstrates that the 6-fluoro substituent is beneficial (5-fold) for affinity (Table 2) and is consistent with the increased affinity imparted by the chloro

Table 3. Enzymatic and Cell-Based Activity of 3 at BACE1 and Related Aspartyl Proteases[a]

	human enzyme K_i [nM]					HEK293 APP$^{Swe/Lon}$ cell IC$_{50}$ [nM]		
BACE1	BACE2	CatD	CatE	pepsin	renin	Aβ1−40	Aβ1−42	sAPPβ
2.2	0.38	≫100,000	≫100,000	≫100,000	33,800	2.1	0.7	4.4

[a]K_i values were determined using purified human aspartyl proteases, and IC$_{50}$ values were determined in HEK293 cells expressing human APP with the Swedish and London familial AD mutations as previously described.[18,21] Data shown represent the mean of 3−5 independent experiments performed in duplicate.

substituent on the thiophene ring of biaryl analogue 7 that we had reported previously.[21] A major advantage of iminothiadiazinane dioxide picolinamides 3 and 29−31 over their iminopyrimidinone counterparts 22−25 was their significantly higher permeabilities and reduced efflux ratios in the Caco-2 assay. Overall permeability values and efflux ratios for 3 and 29−31 approached those of the biaryl analogues 7 and 9. This translated into robust activity in the acute rat pharmacodynamic screen, where the fluoro- and chloropicolinamides 3 and 30 elicited substantial CSF and cortex Aβ40 lowering that was greater than that observed for the corresponding iminopyrimidinones 23 and 24. Further characterization of iminothiadiazinane dioxide 3 and corresponding iminopyrimidinone 23 in LLC-PK1 cells transfected with MDR1, an assay that is more sensitive than the Caco-2 assay for the detection of Pgp substrates, demonstrated that both compounds are Pgp substrates. In LLC-MDR1 cells, iminothiadiazinane dioxide 3 (P_{app} = 29 × 10^{-6} cm sec^{-1}; efflux ratio = 11) had higher permeability and a lower efflux ratio than those of 23 (P_{app} = 19 × 10^{-6} cm sec^{-1}; efflux ratio > 29), consistent with the trends observed in the Caco-2 assay. The excellent permeability conferred by the iminothiadiazinane ring likely accounts for the robust CNS pharmacodynamic activity of 3 and its analogues and is sufficient to overcome Pgp-mediated efflux. The higher overall permeability observed for the iminothiadiazinane dioxide picolinamides compared to the corresponding iminopyrimidinones is ascribed to the weaker basicity of the iminothiadiazinane dioxide core as reported for structurally related BACE1 inhibitors.[25] The lower pK_a of the iminothiadiazinane core may also contribute to reduced Pgp efflux susceptibility, consistent with reports for structurally unrelated compounds.[35] Accordingly, the pK_a of iminothiadiazinane dioxide 3 was determined to be 7.5, significantly lower than that of the corresponding iminopyrimidinone 23 (8.3).

Comparison of 5-chloropyridine derivative 30 (previously reported as MBi-3)[36] with corresponding benzamide 32 highlights the profoundly beneficial effects of the pyridine nitrogen with respect to BACE1 affinity and efflux susceptibility. The reduced permeability and higher efflux ratio of the benzamide 32 can be attributed to the lack of an internal H-bond to the amide hydrogen, effectively unmasking the amide H-bond donor. The loss of affinity is likely a consequence of the difference in conformational bias of the benzamide relative to the picolinamide, which in the case of the benzamide 32 disfavors the near-planar bioactive conformation of the picolinamide motif (vide infra).[37]

■ PRECLINICAL CHARACTERIZATION

5-Fluoropyridine analogue 3 was selected for detailed characterization with key in vitro potency and selectivity data detailed in Table 3.[38] In a cell-based assay, 3 potently inhibits both Aβ40 and Aβ42 formation with similar IC$_{50}$ values. A similar cell-based IC$_{50}$ value is also observed for inhibition of sAPPβ, one of the direct products of BACE1 cleavage of APP. In addition

to its lack of inhibition of CatD in vitro, 3 does not significantly inhibit cathepsin E (CatE), pepsin, or renin. Compound 3 is a potent inhibitor of the BACE1 homologue BACE2 (K_i = 0.38 nM), which is not unexpected given the similarity of the S1 and S3 pockets of the two aspartyl proteases.[39]

The X-ray cocrystal structure of 3 bound to BACE1 shown in Figure 9A confirms a number of specific enzyme−inhibitor
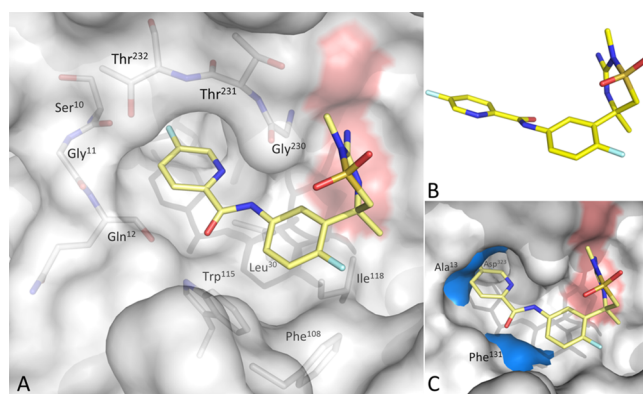
Figure 9. (A) Cocrystal structure of 3 and BACE 1 (PDB: 5HU1). (B) X-ray structure of 3. (C) Cocrystal structure of 3 and BACE1 overlaid with CatD X-ray structure (PDB: 1LYB). CatD residues Phe^{131} and Asp^{323} are highlighted in blue.

interactions. The two H-bond donors of the iminothiadiazinane dioxide core are hydrogen-bonded to the Asp^{32} and Asp^{228} active site residues, and the phenyl group projects pseudoaxially from the thiadiazine core to occupy the hydrophobic S1 pocket defined by Leu^{30}, Phe^{108}, Trp^{115}, and Ile^{118}. The amide exists in the energetically preferred E-configuration, and the amide hydrogen is within H-bonding distance of the Gly^{230} carbonyl oxygen. The two aryl rings are essentially planar with the fluoropyridine substituent positioned between the two loops comprised of Ser^{10}, Gly^{11} and Gln^{12} and Gly^{230}, Thr^{231} and Thr^{232} that define the S3 pocket. The pyridine fluoro substituent extends into the S3 subpocket and is in close proximity to the Ala^{335} methyl side chain (not shown).

The small molecule X-ray crystal structure of 3 (Figure 9B) recapitulates the key conformational features of the verubecestat bioactive conformation defined by the BACE1-bound inhibitor structure (Figure 9A). These include the conformation of the iminothiadiazinane dioxide ring and the pseudoaxial disposition of the fluorophenyl substituent, the E amide orientation, and the position of the pyridine nitrogen to form an internal H-bond to the amide hydrogen. A conformational search on 3 confirmed that the crystal structures of 3 correspond to low energy conformations with the pseudoaxial conformation of the core phenyl substituent enforced by the quaternary methyl group and the internal hydrogen bond locking the conformation of the picolinamide, effectively limiting the number of rotatable bonds to two.

Insight into the lack of affinity of **3** for CatD is provided by comparison of the S1−S3 pockets of CatD and BACE1 (Figure 9C). Binding of **3** to CatD should be disfavored by a close contact of the amide carbonyl of **3** with the S1 Phe[131] residue. Moreover, S3 and S3[sp] of CatD are smaller than the corresponding BACE1 pockets with Ala[13] (S3) and Asp[323] (S3[sp]) of CatD unable to accommodate the steric demand of the fluoropyridyl group of **3**.[33] Rotation of the pyridyl group to alleviate steric clashes within S3 of CatD would be disfavored due to disruption of the energetically preferred planar picolinamide conformation of the inhibitor.

There is a notable discrepancy between the robust CNS activity of **3** (vide infra) and the compound's high calculated polar surface area (115 Å^2),[26] which is beyond the upper limit of 90 Å^2 suggested for CNS active drugs.[40] The internal H-bond between the pyridine nitrogen and the amide hydrogen effectively masks the polarity of these groups,[41] reducing the solvent accessible surface area and hence the dehydration penalty necessary to achieve efficient cell membrane permeability and blood-brain barrier permeation. The high permeability of **3** is sufficient to mitigate the effects of Pgp-mediated efflux. The importance of the internal hydrogen bond to the CNS drug-like properties of the series is reinforced by the observation that its removal through replacement of the pyridyl with phenyl reduces permeability and increases Pgp efflux susceptibility (cf. **30** and **32** in Table 2).

The pharmacokinetic-pharmacodynamic profile of **3** was more fully characterized in rats and cynomolgus monkeys. In rats, acute oral administration of **3** dose-dependently reduced CSF and cortex Aβ40 with ED$_{50}$ values of 5 and 8 mg/kg, respectively, corresponding to unbound plasma EC$_{50}$ values of 48 and 81 nM, respectively. Plasma levels of **3** increased in a dose-proportional manner, whereas increases in CSF and total brain exposure were less than dose proportional.[38]

Compound **3** was also evaluated in a time course study in cisterna magna-cannulated cynomolgus monkeys at oral doses of 3 and 10 mg/kg (Figure 10). CSF Aβ40 levels were
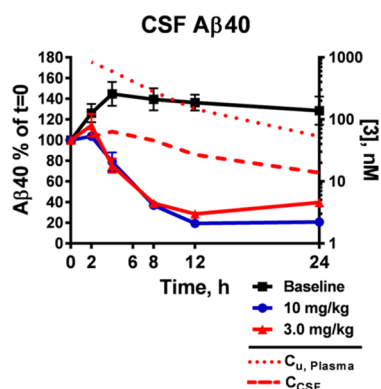
Figure 10. Time course of changes in CSF Aβ40 and concentrations of **3** (3 mg/kg dose) in plasma (unbound) and CSF in cynomolgus monkeys following single oral doses of **3**.

monitored via sequential CSF sampling for 24 h after administration of **3**. Profound, sustained reduction of CSF Aβ40 levels was observed at each dose. Peak effects of **3** on CSF Aβ lowering (72 and 81% reduction at 3 and 10 mg/kg, respectively) were observed 12 h after dosing, which was significantly delayed from the T_{max} of 2 and 6 h for concentrations of **3** in plasma and CSF, respectively. We

attribute this delay in response of CSF Aβ levels to the kinetics of CSF Aβ turnover and to the time required for transit of newly synthesized Aβ from the brain parenchyma to the CSF. This is consistent with results from a separate experiment in which a 10 mg/kg oral dose of **3** to cynomolgus monkeys afforded greater reduction of brain Aβ levels (72%) compared to CSF Aβ levels (60%) 4 h postdose.[38] Of note, in the cisterna magna-cannulated monkey study, CSF levels of **3** were significantly lower than unbound plasma levels with $C_{CSF}/C_{u,plasma}$ ranging from 0.1 to 0.6. These ratios increased over time and were consistent between the two dose levels. The observation that CSF levels of **3** deviate from the unbound plasma concentration is consistent with susceptibility of **3** to Pgp-mediated efflux. Despite the susceptibility to transport by Pgp, these acute pharmacodynamic studies demonstrated that **3** achieves central BACE1 inhibition that translates to robust brain Aβ reduction.[38]

The pharmacokinetic properties of **3** were evaluated in Sprague−Dawley (SD) rats, cynomolgus monkeys, and beagle dogs (Table 4).[38] Compound **3** exhibited good to excellent oral bioavailability, low to moderate clearance, and moderate to high volume of distribution. The compound had a high plasma unbound fraction across preclinical species and a comparable human plasma unbound fraction (45%). Fixed exponent allometric scaling of the rat, dog, and monkey PK parameters predicted a human plasma $t_{1/2}$ of 11 h for **3**, consistent with QD dosing in the clinic.[42] Human dose predictions employed an E_{max} concentration−response model and predicted a human QD dose of 35 mg to achieve a steady-state AUC$_{24h}$ Aβ40 reduction of 75% based on the monkey brain and CSF Aβ40 pharmacodynamic profile.[38] The predicted unbound plasma C_{max} of **3** required to achieve this effect was 82 nM. The crystalline free base of **3** has excellent aqueous solubility (1.6 mM), was selected as the development form, and was predicted to be a BCS class 1 substance at projected clinical doses.

Metabolism of **3** was evaluated in human hepatocytes resulting in identification of two metabolites: *N*-2 desmethyl metabolite **33** and aniline metabolite **34** (Figure 11). Each of these metabolites had BACE1 inhibitory activity that was >100-fold less than that of **3**. In vivo, **33** and **34** were observed as circulating metabolites following oral administration of **3** to rats and monkeys. Aniline **34** was not mutagenic in a 5-strain Ames test.

Many BACE inhibitors including **3** display a basic moiety situated in proximity to a hydrophobic group, a pharmacophore that is also recognized by the I$_{KR}$ channel encoded by the human Ether-A-Go-Go gene (hERG).[43] Inhibition of the hERG channel is implicated in QT prolongation, which can lead to cardiac arrhythmia and sudden death.[44] In vitro, **3** was determined to have an IC$_{50}$ value for inhibition of the hERG channel of 2.2 μM, 27-fold higher than the projected human unbound C_{max} of 82 nM. In a single-dose cardiovascular study in telemetered cynomolgus monkeys, **3** had no effect on the QT interval at an unbound plasma concentration of 1.5 μM, which is approximately 18-fold higher than the predicted human unbound C_{max}.

Compound **3** does not significantly inhibit human CYP isoforms 1A2, 2C9, 2C19, 2D6, and 3A4 (all IC$_{50}$ > 40 μM), indicating that the compound is unlikely to be a perpetrator of CYP-mediated drug−drug interactions. Additionally, **3** at concentrations up to 15 μM did not induce CYP 3A4 or 1A2 expression in human hepatocytes. To further examine the potential of **3** for liver enzyme induction, the compound was

Table 4. Pharmacokinetic Parameters of 3 in SD Rat, Beagle Dog, and Cynomolgus Monkey

	IV administration[a]				oral administration (3 mg/kg)[b]			
	dose [mg kg^{-1}]	Cl [mL min^{-1} kg^{-1}]	V_{dss} [L kg^{-1}]	$t_{1/2}$ [h]	AUC [μM h]	C_{max} [μM]	F [%]	plasma f_u [%]
rat	3	46	5.4	1.9	1.1	0.27	45	37
monkey	1	21	7.5	4.9	5.7	0.60	95	50
dog	1	4.3	2.7	9.7	42	1.6	100	36

[a]Dosed as a solution of the HCl salt in 20% hydroxypropyl-β-cyclodextrin. [b]Dosed as a solution of the HCl salt in 0.4% hydroxypropyl methylcellulose.
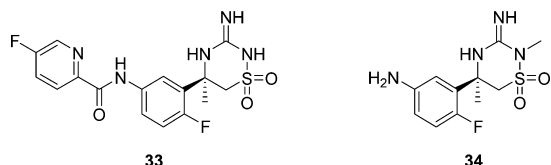

Figure 11. Metabolites of 3.

administered orally at a dose of 30 mg/kg BID for 5 days to rats. This subchronic administration of 3 caused a modest (1.4-fold) induction of CYP 3A1 activity but did not significantly alter the expression of CYPs 1A1, 1A2, 2B, 3A2, or 4A. There was also no effect of subchronic administration of 3 on liver weights. In contrast, subchronic administration of the iminopyrimidinone congener 23 (30 mg/kg BID, 5 days) caused significant induction of CYPs 1A, 2B, and 3A1, liver weight gain, and autoinduction as evidenced by a 3-fold decrease in plasma levels on day 5, thus revealing an

unexpected difference in properties manifested by alteration of the iminoheterocycle core.

In chronic toxicology studies in rats (doses up to 75 mg kg^{-1} day^{-1} for 6 months) and monkeys (doses up to 100 mg kg^{-1} day^{-1} for 9 months), 3 did not elicit neurodegeneration or lipofuscinosis in the CNS consistent with its high selectivity for BACE1 over CatD (>45,000-fold), nor did it alter the histomorphological profile of sciatic or CNS nerve myelination.[38] As mentioned previously, 3 is a potent inhibitor of BACE2. Although knowledge of the specific functions of BACE2 is evolving, recent reports have demonstrated that BACE2 processes the melanosome structural protein PMEL17, which is required for proper pigmentation and is consistent with the lighter coat color observed in Bace2 knockout mice.[45] In addition, it has been postulated that BACE2 plays a role in the function of pancreatic β cells through processing of the transmembrane protein Tmem27. Bace2 knockout mice display improved glucose homeostasis, and Bace2 inhibition has been reported to produce beneficial effects on glucose homeostasis

Scheme 1. Synthesis of Iminothiadiazinane Dioxide 9[a]
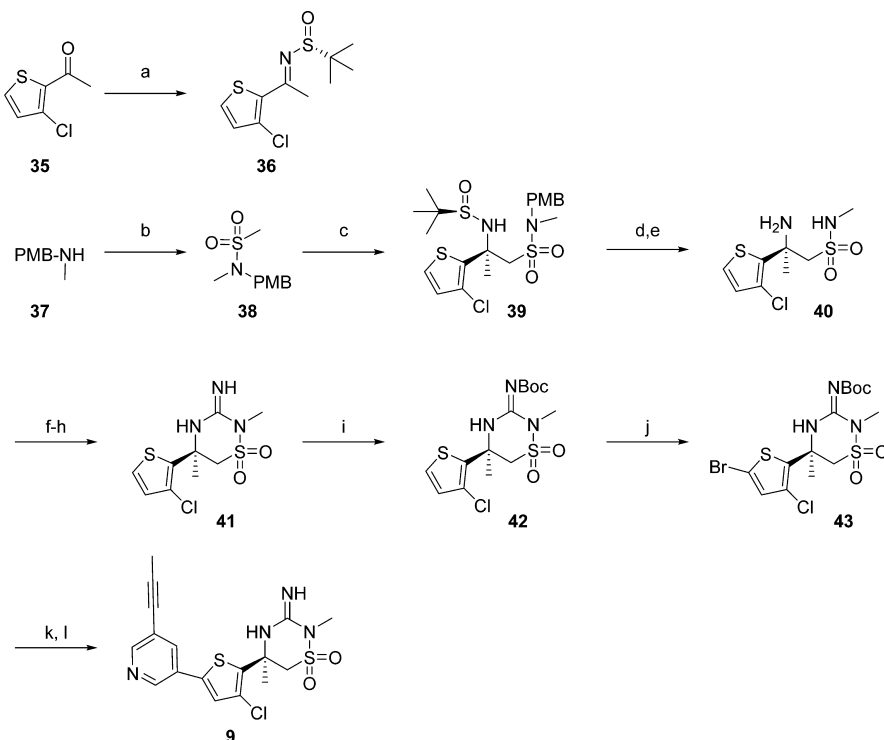
[a]Reagents and conditions: (a) (R)-2-methylpropane-2-sulfinamide, Ti(OEt)$_4$, THF, reflux, 61%; (b) MsCl, Et$_3$N, CH$_2$Cl$_2$, rt, 90%; (c) n-BuLi, THF −78 °C; 36, THF, −78 °C, 75%; (d) 4 N HCl in dioxane, MeOH, CH$_2$Cl$_2$, rt; (e) TFA, 1,3-dimethoxybenzene, CH$_2$Cl$_2$, rt. 99% (crude, 2 steps); (f) benzoylisothiocyanate, CH$_2$Cl$_2$, rt; (g) NaOMe, MeOH, rt; (h) MeI, EtOH, reflux, 81% (3 steps); (i) di-tert-butyldicarbonate, Et$_3$N, CH$_2$Cl$_2$, rt, 72%; (j) NBS, DMF, 50 °C, 63%; (k) (5-(prop-1-ynyl)pyridin-3-yl)boronic acid, 2 M Na$_2$CO$_3$, PdCl$_2$(dppf)·CH$_2$Cl$_2$, 1,4-dioxane, 65 °C; di-tert-butyldicarbonate, Et$_3$N, CH$_2$Cl$_2$; (l) CF$_3$CO$_2$H, CH$_2$Cl$_2$, rt, 21% (3 steps).

Scheme 2. Synthesis of Iminopyrimidinone Amides 21−25[a]
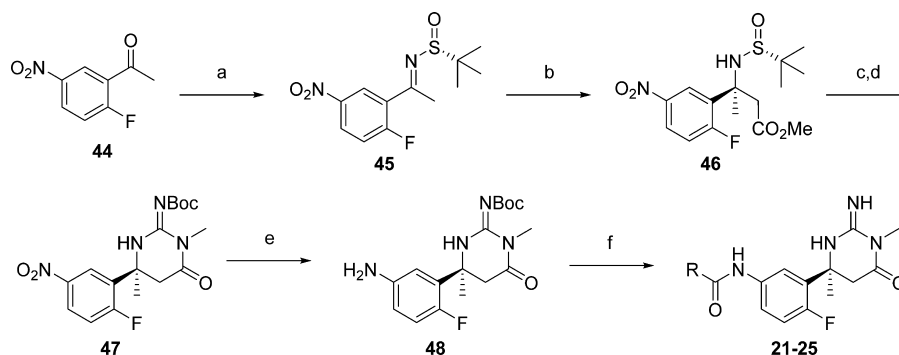
[a]Reagents and conditions: (a) (R)-2-methylpropane-2-sulfinamide, Ti(OEt)$_4$, THF, reflux, 64%; (b) LDA, methyl acetate, ClTi(O^{i}Pr)$_3$, THF, −78 °C; **45**, THF, −78 °C, 75%; (c) HCl, 1,4-dioxane, rt; (d) EDCI, N-[(methylamino)thioxomethyl]-t-butylcarbamate, ^{i}Pr$_2$NEt, THF, rt, 49% (2 steps); (e) H$_2$, Pd/C, MeOH, rt, 94%; (f) RCO$_2$H, BOPCl, pyr, rt; (g) CF$_3$CO$_2$H, CH$_2$Cl$_2$, rt, 23−89% (2 steps).

Scheme 3. Synthesis of Iminothiadiazinane Dioxide Amides 3 and 28−32[a]
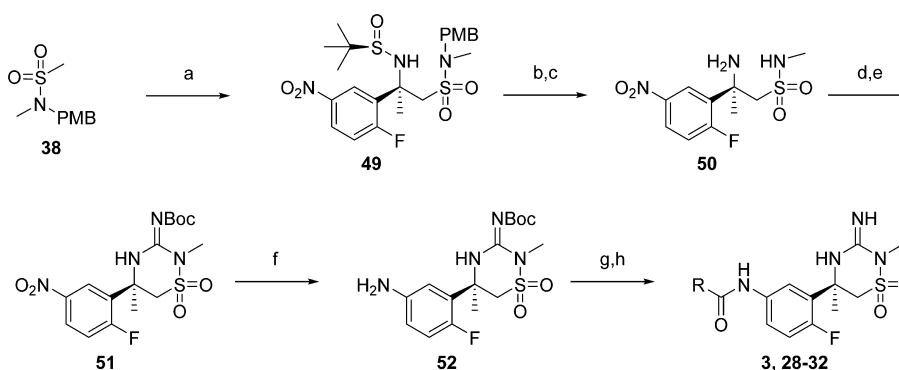
[a]Reagents and conditions: (a) n-BuLi, THF, −78 °C, **45**; THF, −78 °C, 56%; (b) 4 N HCl in 1,4-dioxane, MeOH, CH$_2$Cl$_2$, rt; (c) TFA, 1,3-dimethoxybenzene, CH$_2$Cl$_2$, rt, 90% (2 steps); (d) 5 M BrCN in MeCN, n-BuOH, reflux; (e) di-tert-butyldicarbonate, Et$_3$N, DCM, rt, 59% (2 steps); (f) H$_2$, Pd/C, EtOH, THF, rt, 90%; (g) RCO$_2$H, BOPCl, pyr, rt; (h) CF$_3$CO$_2$H, CH$_2$Cl$_2$, rt, 35−89% (2 steps).

and increased pancreatic β-cell mass in ob/ob mice.[46] Fur hypopigmentation was observed in mice and rabbits treated with **3**; however, in the aforementioned monkey chronic toxicology study, there was no evidence of fur hypopigmentation or changes in pigmentation of any tissue. In addition, no changes in blood glucose levels were observed in chronic rat and monkey studies.[38] Overall, the relatively benign phenotypes of Bace knockout mice, current understanding of the role of BACE2 processing of its endogenous substrates, and the outcome of preclinical toxicology studies has mitigated concerns related to the lack of selectivity of **3** over BACE2.

CLINICAL EVALUATION

The safety, pharmacokinetics, and pharmacodynamics of **3** were assessed in Phase 1 clinical trials in healthy volunteers and mild-to-moderate AD patients.[38] In healthy volunteers, single oral doses of **3** up to 550 mg were safe and well tolerated. Plasma and CSF levels of **3** increased in a dose-proportional manner, and the terminal plasma half-life was 14−24 h. Compound **3** elicited dose-dependent reductions of CSF Aβ40, Aβ42, and sAPPβ with >90% reduction of CSF Aβ40 achieved at the 550 mg dose. Additionally, no QTc prolongation was observed in healthy volunteers administered daily oral doses of **3** at or below the supratherapeutic dose of 250 mg for 14 days. In a Phase 1b study of **3** in patients with mild to moderate AD, oral doses of 12, 40, and 60 mg once per day for 7 days resulted in sustained dose-dependent reductions of CSF Aβ40, Aβ42, and

sAPPβ. Mean reduction of each CSF analyte was >80% at the 60 mg dose. Notably, there were no reports of changes in skin or hair pigmentation as a potential consequence of BACE2 inhibition in any of the Phase 1 studies; however, treatment time of longer duration would likely be required for pigmentation changes to manifest. Compound **3** is currently under evaluation in Phase 3 clinical trials in prodromal and mild to moderate AD patients at doses of 12 and 40 mg. These doses were selected on the basis of simulations of the Phase 1 pharmacodynamic data, which predicted that 95% of patients will achieve CSF Aβ peptide reductions of >50 and >75% at the 12 and 40 mg doses, respectively.[38]

CHEMISTRY

Synthesis of iminothiadiazinane dioxide **9** (Scheme 1) began with treatment of (R)-tert-butylsulfinyl ketimine **36**, readily available from ketone **35**, with the conjugate base of sulfonamide **38** made from commercial 1-(4-methoxyphenyl)-N-methylmethanamine **37**. This process generated the protected β-amino sulfonamide **39** in 75% yield and high diastereomeric ratio (dr 98:2).[47,48] The tert-butylsulfinamide group was cleaved upon treatment of adduct **39** with hydrogen chloride, and the p-methoxy benzyl (PMB) group was subsequently removed using TFA to afford β-amino sulfonamide **40**. The iminothiadiazinane dioxide core was then formed in high yield using a three step protocol.[49] First, treatment of amine **40** with benzoylisothiocyanate was followed

by cleavage of the benzoyl group to provide an intermediate thiourea. Activation of the thiourea with methyl iodide induced an intramolecular ring closure to provide iminothiadiazinane dioxide **41**. Protection of the guanidine with a Boc group provided **42**, which was followed by regioselective bromination of the thiophene ring to afford key intermediate **43**. A Suzuki coupling between **43** and (5-(prop-1-ynyl)pyridin-3-yl)boronic acid and subsequent Boc deprotection provided biaryl iminothiadiazinane dioxide **9**.

Scheme 2 describes the preparation of the iminopyrimidinone amides **21−25**. The iminopyrimidinone core was prepared in a similar fashion to our previously described chemistry.[21] Ketimine **45**, derived from methyl ketone **44**, was subjected to an asymmetric aldol addition with the enolate of methyl acetate providing the β-amino ester **46**. Sulfinamide cleavage under acidic conditions was followed by addition of the resultant amine to *N*-[(methylamino)thioxomethyl]-*t*-butylcarbamate. Subsequent ring closure afforded the iminopyrimidinone core, which was Boc protected to provide **47**. Nitro reduction was followed by amide coupling with a set of pyridine carboxylic acids and Boc deprotection to provide the iminopyrimidinone carboxamide analogues **21−25**.

The iminothiadiazinane dioxide amides **3** and **28−32** were prepared using a modified route (Scheme 3) compared to that described for the preparation of **9**. The addition of the lithium anion of sulfonamide **38** to ketimine **45** afforded amino sulfonamide **49** in 64% yield in a diastereomeric ratio of 93.5:6.5 favoring the desired *R,R* diastereomer. The minor diastereomer was easily removed by silica gel column chromatography. After acidic cleavage of the sulfinamide and PMB groups to afford the β-amino sulfonamide derivative **50**, the iminothiadiazinane dioxide ring was formed in a single step using cyanogen bromide in moderate yield. The previously described three step protocol employing benzylisothiocyanate afforded the desired thiadiazinane as well; however, the yields were poor, and the reproducibility was inconsistent due to multiple side products formed via aromatic nucleophilic substitution on the nitro-activated fluorobenzene moiety. After thiadizininane ring formation, the guanidine was Boc-protected to afford **51**, which was followed by nitro reduction to afford aniline **52**. Finally, amide formation and deprotection afforded the heterocyclic iminothiadiazinane dioxide amides **3**[50] and **28−32**.

CONCLUSIONS

In this work, we have established the novel iminothiadiazinane dioxide core as a viable BACE1 catalytic dyad binding motif and have applied this innovative core to develop novel BACE1 inhibitors with favorable CNS drug-like properties. These efforts have culminated in the discovery of compound **3**, which incorporates key structural features that are critical for fine-tuning its properties into ranges that provide robust central pharmacodynamic activity and minimize undesirable off-target activities. Efflux susceptibility and permeability of **3** are favorably modulated by the reduced basicity of the iminothiadiazinane dioxide core relative to the iminopyrimidinone core and by the presence of an intramolecular hydrogen bond between the pyridine and amide hydrogen. The importance of the *N*-phenylpicolinamide S1−S3 binding motif is underscored by the high BACE1 affinity and CatD selectivity that this structural feature imparts when combined with the iminothiadiazinane dioxide core. Oral administration of **3** elicits robust reduction of centrally derived Aβ40 in

preclinical species, which translated to profound reductions of CSF Aβ peptides in healthy volunteers and AD patients. Compound **3** is a first-in-class BACE1 inhibitor that has advanced to Phase 3 trials in mild to moderate AD and prodromal AD and presents a unique opportunity to provide a robust test of the amyloid hypothesis.

EXPERIMENTAL SECTION

Synthetic Materials and Methods. Reagents and solvents were obtained from commercial sources and used without further purification. ¹H NMR spectra (400 and 500 MHz) were collected on Varian spectrometers. Chemical shifts are reported in ppm relative to the residual solvent peak in the indicated solvent, and for ¹H NMR spectra, multiplicities, coupling constants in hertz, and numbers of protons are indicated parenthetically. Optical rotations were determined using a PerkinElmer model 341 polarimeter, and substrate concentration c is reported in g/100 mL. Purities of all reported compounds were greater than 95% based on HPLC chromatograms obtained on an Agilent 1100 LCMS system.

(R)-N-(1-(3-Chlorothiophen-2-yl)ethylidene)-2-methylpropane-2-sulfinamide (36). To a solution of 1-(3-chlorothiophen-2-yl)ethanone (**35**) (10 g, 62 mmol) in THF (40 mL) were added (*R*)-2-methylpropane-2-sulfinamide (7.9 g, 65 mmol) followed by titanium(IV)ethoxide (13 g, 69 mmol). The resultant mixture was heated to reflux and stirred for 16 h. After that time, the mixture was cooled to room temperature and poured into ice water, and the mixture was filtered. The filter cake was washed with CH₂Cl₂, and the combined filtrates were then extracted with CH₂Cl₂. The combined organic layers were dried over Na₂SO₄, filtered, and concentrated in vacuo. The crude residue was purified by flash chromatography (SiO₂; gradient elution 0−35% EtOAc in hexanes) to afford **36** (10 g, 61% yield) as a yellow solid. ¹H NMR (400 MHz, CDCl₃) δ 7.40 (d, *J* = 5.6 Hz, 1H), 6.96 (d, *J* = 5.6 Hz, 1H), 2.88 (s, 3H), 1.30 (s, 9H).

N-(4-Methoxybenzyl)-N-methylmethanesulfonamide (38). To a solution of 1-(4-methoxyphenyl)-*N*-methylmethanamine (**37**) (10.1 g, 66.8 mmol) in CH₂Cl₂ (100 mL) at 0 °C were added Et₃N (12.1 mL, 86.4 mmol) followed by the dropwise addition of methanesulfonyl chloride (5.95 mL, 76.8 mmol). The mixture was stirred at 0 °C for 30 min and then allowed to warm to room temperature with stirring for an additional 16 h. After that time, the mixture was diluted with CH₂Cl₂ and washed with 1 N HCl(aq) and sat. NaHCO₃(aq). The organic layer was then dried over Na₂SO₄, filtered, and concentrated in vacuo. The crude residue was purified by flash chromatography (SiO₂; gradient elution 0−50% EtOAc in hexanes) to afford **38** (13.8 g, 90% yield) as an off white solid. ¹H NMR (400 MHz, CDCl₃) δ 7.27 (d, *J* = 8.0 Hz, 2H), 6.90 (d, *J* = 8.0 Hz, 2H), 4.25 (s, 3H), 3.81 (s, 2H), 2.81 (s, 3H), 2.75 (s, 3H). ESI MS *m/z* 252.0 [M + Na]⁺.

(S)-2-(3-Chlorothiophen-2-yl)-2-((R)-1,1-dimethylethylsulfinamido)-N-(4-methoxybenzyl)-N-methylpropane-1-sulfonamide (39). To a flame-dried round-bottom flask containing a solution of **38** (7.8 g, 34 mmol) in THF (75 mL) at −78 °C under an atmosphere of nitrogen was added dropwise a solution of *n*-BuLi (1.6 M in hexanes, 21 mL, 34 mmol), and the mixture was stirred for 30 min. After that time, the solution was transferred by cannula a precooled solution (−78 °C) of ketimine **36** (4.0 g, 15 mmol) in THF (75 mL). The resultant mixture was stirred at −78 °C for 5 h. After that time, the mixture was quenched with water and allowed to warm to room temperature. The mixture was then extracted with EtOAc (3×). The combined organic layers were dried over Na₂SO₄, filtered, and concentrated in vacuo. The crude residue was purified by flash chromatography (SiO₂; gradient elution 0−70% EtOAc in hexanes) to afford **39** (5.6 g, 75% yield). ¹H NMR (400 MHz, CDCl₃) δ 7.24−7.18 (m, 3H), 6.96 (d, *J* = 6.0 Hz, 1H), 6.85 (d, *J* = 8.8 Hz, 2H), 6.36 (s, 1H), 4.21 (d, *J* = 14.0 Hz, 1H), 4.17 (s, 2H), 3.79 (s, 3H), 3.68 (d, *J* = 14.0 Hz, 1H), 2.71 (s, 3H), 1.99 (s, 3H), 1.34 (s, 9H). ESI MS *m/z* 493.08 [M + H]⁺.

(S)-2-Amino-2-(3-chlorothiophen-2-yl)-N-methylpropane-1-sulfonamide (40). To a solution of **39** (5.6 g, 11 mmol) in a mixture

of CH$_2$Cl$_2$:MeOH (3:1, 50 mL) at room temperature was added a solution of HCl (4 N in dioxane, 17 mL, 68 mmol). The mixture was stirred at room temperature for 1 h. After that time, the mixture was concentrated in vacuo, and the resultant residue was treated with toluene (100 mL) and concentrated in vacuo again. To the obtained residue were added CH$_2$Cl$_2$ (50 mL) followed by TFA (26 mL, 341 mmol) and 1,3-dimethoxybenzene (10 mL, 80 mmol). The reaction mixture was stirred at room temperature for 16 h. After that time, the volatiles were removed in vacuo, and 1 M HCl(aq) was added to the mixture, which was then extracted with Et$_2$O (3×). The aqueous layer was then adjusted to pH ∼10 with the addition of sat. Na$_2$CO$_3$(aq). The aqueous layer was then extracted with CH$_2$Cl$_2$ (3×). The combined organic layers were dried over Na$_2$SO$_4$, filtered, and concentrated in vacuo to afford **40** (3.0 g, 99% crude yield), which was carried on without further purification. ^{1}H NMR (400 MHz, CDCl$_3$) δ 7.15 (d, J = 5.2 Hz, 1H), 6.90 (d, J = 5.2 Hz, 1H), 4.36 (br s, 1H), 3.94 (d, J = 14.4 Hz, 1H), 3.45 (d, J = 14.4 Hz, 1H), 2.66 (s, J = 5.2 Hz, 3H), 2.49 (br s, 2H), 1.76 (s, 3H). ESI MS m/z 269.2 [M + H]$^+$.

(S)-5-(3-Chlorothiophen-2-yl)-3-imino-2,5-dimethyl-1,2,4-thiadiazinane 1,1-dioxide (41). To a solution of **40** (3.0 g, 11 mmol) in CH$_2$Cl$_2$ (50 mL) was added benzoylisothiocyanate (1.8 mL, 13 mmol), and the mixture was stirred at room temperature overnight. After that time, the volatiles were removed in vacuo. To the residue was added MeOH (50 mL) followed by a solution of sodium methoxide (25% in MeOH, 6.4 mL, 28 mmol). The mixture was stirred at room temperature for 45 min after which the solvent was removed in vacuo. The residue was partitioned between CH$_2$Cl$_2$ and water, and the aqueous layer was adjusted to pH ∼8 with the addition of 1 N HCl(aq) and sat. NaHCO$_3$(aq). The aqueous layer was then extracted with CH$_2$Cl$_2$ (3×). The combined organic layers were dried over Na$_2$SO$_4$, filtered, and concentrated in vacuo to afford the crude intermediate thiourea. To the thiourea were added EtOH (50 mL) followed by methyl iodide (0.84 mL, 13 mmol), and the mixture was heated to reflux with stirring for 8 h. The mixture was then cooled to room temperature, and the solvent was removed in vacuo. The residue was partitioned between water and CH$_2$Cl$_2$. The aqueous layer was basified (pH >9) with sat. Na$_2$CO$_3$(aq). The layers were separated, and the aqueous layer was extracted with CH$_2$Cl$_2$ (2×). The combined organic layers were dried over Na$_2$SO$_4$, filtered, and concentrated in vacuo. The crude residue was purified by flash chromatography [SiO$_2$; gradient elution 0−5% MeOH (with 10% concn NH$_4$OH) in CH$_2$Cl$_2$] to afford **41** (2.6 g, 81% yield) as an off white solid. ^{1}H NMR (400 MHz, DMSO-d$_6$) δ 7.38 (d, J = 5.2 Hz, 1H), 6.93 (d, J = 5.2 Hz, 1H), 6.06 (br s, 2H), 3.91 (s, 2H), 3.04 (s, 3H), 1.62 (s, 3H). ESI MS m/z 294.2 [M + H]$^+$.

(S)-tert-Butyl (5-(3-Chlorothiophen-2-yl)-2,5-dimethyl-1,1-dioxido-1,2,4-thiadiazinan-3-ylidene)carbamate (42). To a solution of **41** (9.6 g, 33 mmol) in THF (100 mL) was added triethylamine (5.5 mL, 39 mmol) and di-tert-butyldicarbonate (8.6 g, 39 mmol), and the resultant mixture was stirred at room temperature for 16 h. After that time, the volatiles were removed in vacuo, and the residue was purified by flash chromatography (SiO$_2$; gradient elution 0−20% EtOAc in hexanes) to afford **42** (9.3 g, 72%) as a white solid. ^{1}H NMR (400 MHz, CDCl$_3$) δ 10.71 (s, 1H), 7.21 (d, J = 6.0 Hz, 1H), 6.96 (d, J = 6.0 Hz, 1H), 4.43 (d, J = 14.0 Hz, 1H), 3.64 (d, J = 14.0 Hz, 1H), 3.28 (s, 3H), 2.02 (s, 3H), 1.52 (s, 9H). ESI MS m/z 394.0 [M + H]$^+$.

(S)-tert-Butyl (5-(5-Bromo-3-chlorothiophen-2-yl)-2,5-dimethyl-1,1-dioxido-1,2,4-thiadiazinan-3-ylidene)carbamate (43). To a solution of **42** (2.2 g, 5.6 mmol) in DMF (60 mL) was added NBS (2.7 g, 15 mmol). The mixture was heated to 50 °C with stirring for 8 h then allowed to cool to rt. The reaction mixture was quenched with sat. Na$_2$S$_2$O$_5$(aq), partioned between water and EtOAc, and the aqueous layer was extracted with EtOAc (3×). The combined organic layers were dried over Na$_2$SO$_4$, filtered, and concentrated in vacuo. The residue was purified by flash chromatography (SiO$_2$; gradient elution 0−17% EtOAc in hexanes) to afford **43** (1.7 g, 63% yield). ^{1}H NMR (400 MHz, CDCl$_3$) δ 10.78 (br s, 1H), 7.26 (s, 1H), 4.48 (d, J = 14.0 Hz, 1H), 3.58 (d, J = 14.0 Hz, 1H), 3.28 (s, 3H), 2.97 (s, 3H), 1.53 (s, 9H). ESI MS m/z 495.8 [M + Na]$^+$.

(S)-5-(3-Chloro-5-(5-(prop-1-yn-1-yl)pyridin-3-yl)thiophen-2-yl)-3-imino-2,5-dimethyl-1,2,4-thiadiazinane 1,1-Dioxide (9). To a vial containing **43** (360 mg, 0.76 mmol) were added [5-(prop-1-yn-1-yl)pyridin-3-yl]boronic acid (210 mg, 1.3 mmol) followed by PdCl$_2$(dppf)·CH$_2$Cl$_2$ (93 mg, 0.11 mmol). The vial was transferred into a glovebox under an atmosphere of nitrogen. To the vial were added t-BuOH (6 mL) followed by an aqueous solution of K$_2$CO$_3$ (2M, 1.1 mL, 2.2 mmol), and the mixture was stirred at 65 °C overnight. After that time, the mixture was cooled to room temperature and filtered. To the filtrate was added water, and the mixture was extracted with CH$_2$Cl$_2$ (3×). The combined organic layers were dried over Na$_2$SO$_4$, filtered, and concentrated in vacuo. To the residue were added CH$_2$Cl$_2$ (6 mL) followed by diisopropylethylamine (0.27 mL, 1.5 mmol) and di-tert-butyldicarbonate (0.18 mL, 0.76 mmol). The mixture was stirred at room temperature for 24 h. The reaction was quenched with water, and the aqueous layer was extracted with CH$_2$Cl$_2$ (3×). The combined organic layers were dried over Na$_2$SO$_4$, filtered, and concentrated in vacuo. The residue was purified by flash chromatography (SiO$_2$; gradient elution 0−40% EtOAc in hexanes) to afford the intermediate Boc carbamate (100 mg, 26% yield) as a white foam. To a solution of this intemediate in CH$_2$Cl$_2$ (1 mL) was added TFA (1 mL). The resultant solution was stirred at room temperature for 2 h. After that time, the soluton was concentrated in vacuo. The crude residue was purified by HPLC (C$_{18}$; gradient elution 10−45% MeCN:water with 0.1% TFA) to afford **9** (80 mg, 82% yield) as the TFA salt. ^{1}H NMR (500 MHz, CDCl$_3$) δ 8.80 (d, J = 2.2 Hz, 1H), 8.61 (d, J = 2.0 Hz, 1H), 7.34 (s, 1H), 4.71 (d, J = 14.2 Hz, 1H), 4.55 (br s, 3 H), 3.76 (d, J = 14.2 Hz, 1H), 3.41 (s, 3H), 2.15 (s, 3H), 2.14 (s, 3H). ESI MS m/z 409.1 [M + H]$^+$. [α]$_D^{20}$ −43.1° (c 0.515, CH$_3$OH).

(R)-N-(1-(2-Fluoro-5-nitrophenyl)ethylidene)-2-methylpropane-2-sulfinamide (45). Ketimine **45** (37.4 g, 64% yield) was prepared from **44** following the procedure used to prepare **36**. ^{1}H NMR (400 MHz, CDCl$_3$) δ 8.54 (dd, J = 6.3, 2.9 Hz, 1H), 8.30 (dd, J = 9.1, 3.5 Hz, 1H), 7.28 (t, J = 9.5 Hz, 1H), 2.79 (d, J = 3.5 Hz, 3H), 1.32 (s, 9H). ESI MS m/z 287.1 [M + H]$^+$.

(R)-2-((R)-1,1-Dimethylethylsulfinamido)-2-(2-fluoro-5-nitrophenyl)-N-(4-methoxybenzyl)-N-methylpropane-1-sulfonamide (49). To a flame-dried round-bottom flask containing a solution of **38** (60.0 g, 262 mmol) in THF (750 mL) at −75 °C under an atmosphere of nitrogen was added over 10 min a solution of n-BuLi (1.6 M in hexanes, 165 mL, 262 mmol), and the mixture was stirred for 30 min. After that time, to the mixture was added a solution of ketimine **45** (50.0 g, 175 mmol) in THF (250 mL). The resultant mixture was stirred at −75 °C for 1 h. After that time, the mixture was slowly warmed to rt over 1 h, and then the reaction was quenched with water and brine. The resultant mixture was then extracted with EtOAc (3×). The combined organic layers were washed with brine, dried over Na$_2$SO$_4$ and MgSO$_4$, filtered, and concentrated in vacuo. The crude residue (HPLC; dr 93.5:6.5) was purified by flash chromatography (SiO$_2$; gradient elution 0−70% EtOAc in hexanes) to afford **49** (50.8 g, 56% yield) as a single diastereomer. ^{1}H NMR (400 MHz, CDCl$_3$) δ 8.55 (m, 1H), 8.22 (m, 1H), 7.18−7.24 (m, 4 H), 6.84 (dd, J = 8.4, 1.2 Hz, 1H), 5.99 (s, 1H), 4.21 (d, J = 14.8 Hz, 2H), 3.86 (d, J = 14.8 Hz, 2H), 3.78 (s, 3H), 2.71 (s, 3H), 1.61 (s, 3H), 1.40 (s, 9H). ESI MS m/z 538.2 [M + Na]$^+$.

(R)-2-Amino-2-(2-fluoro-5-nitrophenyl)-N-methylpropane-1-sulfonamide (50). Amine **50** (15.5 g, 90% yield) was prepared from **49** following the procedure used to prepare **40**. ^{1}H NMR (400 MHz, CDCl$_3$) δ 8.60 (dd, J = 7.2, 2.4 Hz, 1H), 8.18 (ddd, J = 7.2, 3.6, 3.6 Hz, 1H), 7.17 (dd, J = 10.4, 9.4 Hz, 1H), 4.33 (br s, 1H), 3.85 (d, J = 16.0 Hz, 1H), 3.41 (d, J = 16.0 Hz, 1H), 2.67 (s, 3H), 2.28 (br s, 2H), 1.62 (s, 3H). ESI MS m/z 292.2 [M + H]$^+$.

(R)-tert-Butyl (5-(2-Fluoro-5-nitrophenyl)-2,5-dimethyl-1,1-dioxido-1,2,4-thiadiazinan-3-ylidene)carbamate (51). To a slurry of **50** (26.2 g, 89.9 mmol) in 1-butanol (300 mL) was added a solution of cyanogen bromide (5 M in MeCN, 19.8 mL, 98.9 mmol), and the mixture was heated to reflux with stirring for 4 h. After that time, the mixture was cooled to room temperature and concentrated in vacuo to approximately 1/3 of the original volume. To the mixture was

then added Et$_2$O (300 mL), and the resultant precipitate was removed by filtration. The precipitate was partitioned between EtOAc and sat. Na$_2$CO$_3$(aq), and the mixture was extracted with EtOAc (3×). The combined organic layers were washed with brine, dried over Na$_2$SO$_4$, filtered, and concentrated in vacuo. To the residue was added CH$_2$Cl$_2$ (300 mL) followed by triethylamine (16.6 mL, 120 mmol) and di-*tert*-butyldicarbonate (22.4 g, 102 mmol). The resultant mixture was stirred at rt for 16 h. The mixture was then diluted with CH$_2$Cl$_2$ and washed with Na$_2$CO$_3$(aq). The layers were separated, and the aqueous layer was extracted with CH$_2$Cl$_2$ (2×). The combined organic layers were dried over Na$_2$SO$_4$, filtered, and concentrated in vacuo. The crude residue was purified by flash chromatography (SiO$_2$; gradient elution 0−40% EtOAc in hexanes) to afford **51** (22.3 g, 59% yield) as a light tan solid. ^{1}H NMR (400 MHz, CDCl$_3$) δ 10.82 (s, 1H), 8.26 (m, 2H), 7.28 (m, 1H), 4.29 (d, *J* = 14.4 Hz, 1H), 3.68 (d, *J* = 14.4 Hz, 1H), 3.23 (s, 3H), 1.90 (s, 3H), 1.56 (s, 9H). ESI MS *m/z* 439.0 [M + Na]$^+$.

(R)-tert-Butyl (5-(5-Amino-2-fluorophenyl)-2,5-dimethyl-1,1-dioxido-1,2,4-thiadiazinan-3-ylidene)carbamate (52). To a hydrogenation vessel containing degassed solution **51** (7.3 g, 18 mmol) in 1:1 EtOH:THF (130 mL) was added 10% Pd/C (1.1 g, 0.52 mmol, 50 wt %/wt H$_2$O). The vessel was sealed, evacuated, and backfilled with nitrogen (3×) and then evacuated again and backfilled with hydrogen (3×). The vessel was pressurized to 55 psi with hydrogen, and the mixture was shaken at room temperature for 4 h. The mixture was then purged with nitrogen, and the catalyst was removed by filtration. The filter cake was washed with 1:1 EtOH:THF, and the filtrate was concentrated in vacuo. The crude residue was purified by flash chromatography (SiO$_2$; gradient elution 0−45% EtOAc in hexanes) to afford **52** (6.1 g, 90% yield) as a white solid. ^{1}H NMR (400 MHz, CDCl$_3$) δ 10.48 (br s, 1H), 6.87 (ddd, *J* = 12.0, 8.4, 1.6 Hz, 1H), 6.60−6.50 (m, 2H), 5.28 (s, 2H), 4.25 (d, *J* = 14.0 Hz, 1H), 3.63 (d, *J* = 14.0 Hz, 1H), 3.22 (s, 3H), 1.83 (s, 3H), 1.53 (s, 9H). ESI MS *m/z* 387.0 [M + H]$^+$.

General Procedure A for the Preparation of Compounds 28−32. To a flask containing **52** (100 mg, 0.26 mmol) were added the requisite carboxylic acid (0.34 mmol) and bis(2-oxo-3-oxazolidinyl)-phosphinic chloride (106 mg, 0.42 mmol) followed by pyridine (1.2 mL). The resultant mixture was stirred at rt for 16 h. After that time, the mixture was partitioned between water and EtOAc. The layers were separated, and the aqueous layer was extracted with EtOAc. The combined organic layers were dried over Na$_2$SO$_4$, filtered, and concentrated in vacuo. The crude residue was purified by flash chromatography (SiO$_2$; gradient elution 0−60% EtOAc in hexanes) to afford the intermediate amide. To a flask containing the amide were added CH$_2$Cl$_2$ (3 mL) followed by TFA (1 mL). The resultant solution was stirred at rt for 2 h. After that time, the solution was concentrated in vacuo and dried further under high vacuum to afford the title compound as the trifluoroacetate salt.

(R)-N-(4-Fluoro-3-(3-imino-2,5-dimethyl-1,1-dioxido-1,2,4-thiadiazinan-5-yl)phenyl)picolinamide (28). Compound **28** (78% yield) was prepared following general procedure A. ^{1}H NMR (400 MHz, CDCl$_3$) δ 11.16 (br s, 1H), 10.09 (s, 1H), 9.50 (br s, 2H), 8.53 (d, *J* = 4.8 Hz, 1H), 8.10 (d, *J* = 7.6 Hz, 1H), 7.92 (dd, *J* = 7.6, 2.8 Hz, 1H), 7.83 (ddd, *J* = 7.6, 1.6, 1.6 Hz, 1H), 7.59 (ddd, *J* = 8.8, 2.8, 2.8 Hz, 1H), 7.45 (ddd, *J* = 7.6, 4.8, 1.6 Hz, 1H), 7.12 (dd, *J* = 12.0, 8.8 Hz, 1H), 4.45 (dd, *J* = 14.8, 2.4 Hz, 1H), 3.82 (d, *J* = 14.8 Hz, 1H), 3.31 (s, 3H), 1.95 (s, 3H). ESI MS *m/z* 392.2 [M + H]$^+$.

(R)-N-(4-Fluoro-3-(3-imino-2,5-dimethyl-1,1-dioxido-1,2,4-thiadiazinan-5-yl)phenyl)-5-methylpicolinamide (29). Compound **29** (35% yield) was prepared following general procedure A. ^{1}H NMR (400 MHz, CDCl$_3$) δ 9.91 (br s, 1H), 8.31 (s, 1H), 8.05 (d, *J* = 8.0 Hz, 1H), 7.91 (dd, *J* = 7.2, 2.8 Hz, 1H), 7.64 (m, 2H), 7.03 (dd, *J* = 11.6, 8.8 Hz, 1H), 3.95 (br s, 2H), 3.90 (d, *J* = 14.0 Hz, 1H), 3.68 (d, *J* = 14.0 Hz, 1H), 3.20 (s, 3H), 2.38 (s, 3H), 1.76 (s, 3H). ESI MS *m/z* 406.2 [M + H]$^+$.

N-[3-[(5R)-3-Amino-5,6-dihydro-2,5-dimethyl-1,1-dioxido-2H-1,2,4-thiadiazin-5-yl]-4-fluorophenyl]-5-fluoro-2-pyridine-carboxamide (3). To a flask containing **52** (3.00 g, 7.76 mmol) were added 5-fluoropicolinic acid (1.64 g, 11.6 mmol) and bis(2-oxo-3-

oxazolidinyl)phosphinic chloride (4.54 g, 17.8 mmol) followed by pyridine (8 mL). The resultant mixture was stirred at rt for 1 h. The mixture was then partitioned between water and EtOAc and filtered, and the layers were separated. The aqueous layer was extracted with EtOAc (2×). The combined organic layers were dried over Na$_2$SO$_4$, filtered, and concentrated in vacuo. The crude residue was purified by flash chromatography (SiO$_2$; gradient elution 0−35% EtOAc in hexanes) to afford the intermediate amide (3.50 g, 87% yield). To a flask containing the amide were added CH$_2$Cl$_2$ (30 mL) followed by TFA (10 mL). The resultant solution was stirred at rt for 2 h. After that time, to the solution was added Et$_2$O (50 mL), and the mixture was poured into hexanes (400 mL). The resultant precipitate was isolated by filtration and dried under high vacuum. The obtained solid was partitioned between EtOAc and sat. Na$_2$CO$_3$(aq). The layers were separated, and the aqueous layer was extracted with EtOAc (2×). The combined organic layers were dried over Na$_2$SO$_4$, filtered, and concentrated in vacuo to afford **3** (2.70 g, 89% yield) as a white solid. ^{1}H NMR (400 MHz, DMSO-*d$_6$*) δ 10.57 (s, 1H), 8.73 (d, *J* = 2.8 Hz, 1H), 8.22 (dd, *J* = 8.8, 4.8 Hz, 1H), 8.03−7.95 (m, 2H), 7.79 (m, 1H), 7.14 (dd, *J* = 11.6, 8.8 Hz, 1H), 6.03 (br s, 2H), 3.78 (s, 1H), 3.34 (s, 1H), 3.05 (s, 3H), 1.61 (s, 3H). ESI MS *m/z* 410.2 [M + H]$^+$. [α]$_D^{20}$ 37.2° (*c* 0.367, CH$_3$OH). To generate its hydrochloride salt, **3** prepared above was added to CH$_2$Cl$_2$ (50 mL) followed by a solution of HCl (2 N in Et$_2$O, 3.6 mL, 7.2 mmol), and the mixture was concentrated in vacuo. The product was slurried in distilled water (50 mL) and lyophilized to afford the HCl monohydrate salt of **3** (2.58 g, 79% yield, 3 steps) as a white solid. ^{1}H NMR (400 MHz, CD$_3$OD) δ 8.59 (d, *J* = 2.8 Hz, 1H), 8.26 (dd, *J* = 8.8, 4.8 Hz, 1H), 8.02 (dd, *J* = 7.6, 2.8 Hz, 1H), 7.82−7.75 (m, 2H), 7.22 (dd, *J* = 12.0, 8.8 Hz, 1H), 4.49 (dd, *J* = 14.4, 0.8 Hz, 1H), 4.30 (d, *J* = 14.4 Hz, 1H), 3.30 (s, 3H), 1.96 (s, 3H). ESI MS *m/z* 410.2 [M + H]$^+$. Anal. Calcd (C$_{17}$H$_{20}$ClF$_2$N$_5$O$_4$S): C, 44.02; H, 4.35; N, 15.10; Cl, 7.64; S, 6.91. Found: C, 43.77; H, 4.32; N, 14.81; Cl, 7.84; S, 7.04.

(R)-5-Chloro-N-(4-fluoro-3-(3-imino-2,5-dimethyl-1,1-dioxido-1,2,4-thiadiazinan-5-yl)phenyl)picolinamide (30). Compound **30** (89% yield) was prepared following general procedure A. ^{1}H NMR (400 MHz, CDCl$_3$) δ 11.28 (br s, 1H), 9.75 (s, 1H), 8.90 (br s, 2H), 8.40 (d, *J* = 2.4 Hz, 1H), 7.96−7.90 (m, 2H), 7.66 (dd, *J* = 8.8, 2.4 Hz, 1H), 7.46 (ddd, *J* = 6.4, 2.8, 2.4 Hz, 1H), 7.11 (dd, *J* = 11.6, 8.8 Hz, 1H), 4.51 (dd, *J* = 14.8, 2.8 Hz, 1H), 3.81 (d, *J* = 14.8 Hz, 1H), 3.34 (s, 3H), 1.95 (s, 3H). ESI MS *m/z* 426.2 [M + H]$^+$.

(R)-N-(4-Fluoro-3-(3-imino-2,5-dimethyl-1,1-dioxido-1,2,4-thiadiazinan-5-yl)phenyl)-5-(trifluoromethyl)picolinamide (31). Compound **31** (41% yield) was prepared following general procedure A. ^{1}H NMR (400 MHz, CDCl$_3$) δ 12.00 (br s, 1H), 10.82 (br s, 1H), 9.62 (s, 1H), 8.71 (s, 1H), 8.08 (dd, *J* = 6.8, 1.6 Hz, 1H), 7.95 (d, *J* = 8.0 Hz, 1H), 7.82 (d, *J* = 8.0 Hz, 1H), 7.20 (m, 1H), 7.06 (dd, *J* = 11.6, 8.8 Hz, 1H), 4.60 (dd, *J* = 14.4, 2.8 Hz, 1H), 3.80 (d, *J* = 14.4 Hz, 1H), 3.42 (s, 3H), 1.96 (s, 3H). ESI MS *m/z* 460.0 [M + H]$^+$.

(R)-4-Chloro-N-(4-fluoro-3-(3-imino-2,5-dimethyl-1,1-dioxido-1,2,4-thiadiazinan-5-yl)phenyl)benzamide (32). Compound **32** (56% yield) was prepared following general procedure A. ^{1}H NMR (400 MHz, CDCl$_3$) δ 10.91 (s, 1H), 9.09 (s, 1H), 8.37 (br s, 2H), 7.75 (m, 1H), 7.65 (m 3H), 7.25 (d, *J* = 8.0 Hz, 2H) 7.07 (dd, *J* = 11.6, 8.8 Hz, 1H), 4.34 (d, *J* = 12.4 Hz, 1H), 3.73 (d, *J* = 12.4 Hz, 1H), 3.03 (s, 3H), 1.83 (s, 3H). ESI MS *m/z* 425.2 [M + H]$^+$.

■ ASSOCIATED CONTENT

❺ Supporting Information

The Supporting Information is available free of charge on the [ACS Publications website](#) at DOI: [10.1021/acs.jmedchem.6b00307](#).

> Synthetic methods and characterization data for compounds ^{3}H-**9**, **12−16**, and **20−27**, molecular modeling details, crystallographic information, and methods for in vitro, in vivo, pharmacodynamic, hydrolytic stability, and pharmacokinetic assays (PDF)
> K_i and IC$_{50}$ values for the compounds (CSV)

Accession Codes

3: 5HU1; **9**: 5HTZ; and **13**: 5HU0.

■ AUTHOR INFORMATION

Corresponding Authors

*Phone: 908-740-4729. E-mail: jack.scott@merck.com.
*Phone: 973-868-2088. E-mail: andy.stamford1@gmail.com.

Present Addresses

■(X.C.): Tandem Laboratories, Ridgefield, Connecticut, USA
●(U.I.): Big Boost Marketing, Hoboken, New Jersey, USA
□(R.A.H.): Charles River Laboratories, Boston, Massachusetts, USA
○(J.M.): Metrohm, New Jersey, USA
▲(M.S.): Momentive Performance Materials, Waterford, New York, USA
◇(J. H.V.): Gilead Sciences, Foster City, California, USA
◆(Y.W.): Tetranov International, Inc., New Brunswick, New Jersey, USA
※(W.J.G.): MedChem Discovery Consulting, Teaneck, New Jersey, USA

Notes

The authors declare no competing financial interest.

■ ABBREVIATIONS USED

AD, Alzheimer's disease; APP, amyloid precursor protein; BACE1, β-site APP cleaving enzyme 1; BACE2, β-site APP cleaving enzyme 2; BCS, biopharmaceutical classification system; Boc, tertiary butoxycarbonyl; CatD, cathepsin D; CatE, cathepsin E; CNS, central nervous system; CSF, cerebrospinal fluid; CYP, Cytochrome P_{450}; ER, efflux ratio; f_u, unbound fraction; hERG, human ether-a-go-go related gene; LE, ligand efficiency; MDR1, multidrug resistance protein 1; P_{app}, apparent permeability; Pgp, P-glycoprotein; PMB, para-methoxybenzyl; p.o., per os (dosed by mouth); SAR, structure–activity relationship; sAPPβ, C-terminally truncated form of amyloid precursor protein; SD, Sprague–Dawley; TFA, trifluoroacetic acid

■ REFERENCES

(1) (a) Wortmann, M. Dementia: a global health priority – highlights from an ADI and World Health Organization report. *Alzheimer's Res. Ther.* **2012**, *4*, 40–43. (b) Alzheimer's Disease International. World Alzheimer Report 2015. http://www.alz.co.uk/research/WorldAlzheimerReport2015.pdf.

(2) Alzheimer's Association. 2015 Alzheimer's disease facts and figures. *Alzheimers Dement.* **2015**, 332–384.

(3) Zemek, F.; Drtinova, L.; Nepovimova, E.; Sepsova, V.; Korabecny, J.; Klimes, J.; Kuca, K. Outcomes of Alzheimer's disease therapy with acetylcholinesterase inhibitors and memantine. *Expert Opin. Drug Saf.* **2014**, *13*, 759–774.

(4) Haass, C.; Selkoe, D. J. Soluble protein oligomers in neurodegeneration: Lesson from the Alzheimer's amyloid β-peptide. *Nat. Rev. Mol. Cell Biol.* **2007**, *8*, 101–112.

(5) (a) Hardy, J.; Selkoe, D. J. The amyloid hypothesis of Alzheimer's disease: Progress and problems on the road to therapeutics. *Science* **2002**, *297*, 353–356. (b) Karran, E.; Mercken, M.; De Strooper, B. The amyloid cascade hypothesis for Alzheimer's disease: an appraisal for the development of therapeutics. *Nat. Rev. Drug Discovery* **2011**, *10*, 698–712.

(6) Tanzi, R. E. The genetics of Alzheimer disease. *Cold Spring Harbor Perspect. Med.* **2012**, *2*, 1–10.

(7) Citron, M. Alzheimer's disease: strategies for disease modification. *Nat. Rev. Drug Discovery* **2010**, *9*, 387–398.

(8) Jonsson, T.; Atwal, J. K.; Steinberg, S.; Snaedal, J.; Jonsson, P. V.; Bjornsson, S.; Stefansson, H.; Sulem, P.; Gudbjartsson, D.; Maloney, J.; Hoyte, K.; Gustafson, A.; Liu, Y.; Lu, Y.; Bhangale, T.; Graham, R. R.; Huttenlocher, J.; Bjornsdottir, G.; Andreassen, O. A.; Jönsson, E. G.; Palotie, A.; Behrens, T. W.; Magnusson, O. T.; Kong, A.; Thorsteinsdottir, U.; Watts, R. J.; Stefansson, K. A mutation in APP protects against Alzheimer's disease and age-related cognitive decline. *Nature* **2012**, *488*, 96–99.

(9) Roberds, S. L.; Anderson, J.; Basi, G.; Bienkowski, M. J.; Branstetter, D. G.; Chen, K. S.; Freedman, S. B.; Frigon, N. L.; Games, D.; Hu, K.; Johnson-Wood, K.; Kappenman, K. E.; Kawabe, T. T.; Kola, I.; Kuehn, R.; Lee, M.; Liu, W.; Motter, R.; Nichols, N. F.; Power, M.; Robertson, D. W.; Schenk, D.; Schoor, M.; Shopp, G. M.; Shuck, M. E.; Sinha, S.; Svensson, K. A.; Tatsuno, G.; Tintrup, H.; Wijsman, J.; Wright, S.; McConlogue, L. BACE knockout mice are healthy despite lacking the primary beta-secretase activity in brain: implications for Alzheimer's disease therapeutics. *Hum. Mol. Genet.* **2001**, *10*, 1317–1324.

(10) Vassar, R.; Kuhn, P.-H.; Haass, C.; Kennedy, M. E.; Rajendran, L.; Wong, P. C.; Lichtenthaler, S. F. Function, therapeutic potential and cell biology of BACE proteases: current status and future prospects. *J. Neurochem.* **2014**, *130*, 4–28.

(11) (a) Vassar, R.; Bennett, B. D.; Babu-Khan, S.; Kahn, S.; Mendiaz, E. A.; Denis, P.; Teplow, D. B.; Ross, S.; Amarante, P.; Loeloff, R.; Luo, Y.; Fisher, S.; Fuller, J.; Edenson, S.; Lile, J.; Jarosinski, M. A.; Biere, A. L.; Curran, E.; Burgess, T.; Louis, J.-C.; Collins, F.; Treanor, J.; Rogers, G.; Citron, M. β-Secretase cleavage of Alzheimer's amyloid precursor protein by the transmembrane aspartic protease BACE. *Science* **1999**, *286*, 735–741. (b) Sinha, S.; Anderson, J. P.; Barbour, R.; Basi, G. S.; Caccavello, R.; Davis, D.; Doan, M.; Dovey, H. F.; Frigon, N.; Hong, J.; Jacobson-Croak, K.; Jewett, N.; Keim, P.; Knops, J.; Lieberburg, I.; Power, M.; Tan, H.; Tatsuno, G.; Tung, J.; Schenk, D.; Seubert, P.; Suomensaari, S. M.; Wang, S.; Walker, D.; Zhao, J.; McConlogue, L.; John, V. Purification and cloning of amyloid precursor protein β-secretase from human brain. *Nature* **1999**, *402*, 537–540. (c) Hussain, I.; Powell, D.; Howlett, D. R.; Tew, D. G.; Meek, T. D.; Chapman, C.; Gloger, I. S.; Murphy, K. E.; Southan, C. D.; Ryan, D. M.; Smith, T. S.; Simmons, D. L.; Walsh, F. S.; Dingwall, C.; Christie, G. Identification of a novel aspartic protease (Asp 2) as β-Secretase. *Mol. Cell. Neurosci.* **1999**, *14*, 419–427. (d) Yan, R.; Bienkowski, M. J.; Shuck, M. E.; Miao, H.; Tory, M. C.; Pauley, A. M.; Brashler, J. R.; Stratman, N. C.; Mathews, W. R.; Buhl, A. E.; Carter, D. B.; Tomasselli, A. G.; Parodi, L. A.; Heinrikson, R. L.; Gurney, M. E. Membrane-anchored aspartyl protease with Alzheimer's disease β-secretase activity. *Nature* **1999**, *402*, 533–537. (e) Lin, X.; Koelsch, G.; Wu, S.; Downs, D.; Dashti, A; Tang, J. Human aspartic protease memapsin 2 cleaves the β-secretase site of β-amyloid precursor protein. *Proc. Natl. Acad. Sci. U. S. A.* **2000**, *97*, 1456–1460.

(12) (a) Oehlrich, D.; Prokopcova, H.; Gijsen, H. J. M. The evolution of amidine-based brain penetrant BACE1 inhibitors. *Bioorg. Med. Chem. Lett.* **2014**, *24*, 2033–2045. (b) Yuan, J.; Venkatraman, S.; Zheng, Y.; McKeever, B. M.; Dillard, L. W.; Singh, S. B. Structure-based design of β-site APP cleaving enzyme 1 (BACE) inhibitors for

the treatment of Alzheimer's disease. disease. *J. Med. Chem.* **2013**, *56*, 4156–4180. (c) Probst, G.; Xu, Y. z. Small-molecule BACE1 inhibitors: a patent literature review (2006 - 2011). *Expert Opin. Ther. Pat.* **2012**, *22*, 511–540.

(13) (a) Willem, M.; Garratt, A. N.; Novak, B.; Citron, M.; Kaufmann, S.; Rittger, A.; DeStrooper, B.; Saftig, P.; Birchmeier, C.; Haass, C. Control of peripheral nerve myelination by the β-Secretase BACE1. *Science* **2006**, *314*, 664–666. (b) Hu, X.; Hicks, C. W.; He, W.; Wong, P.; Macklin, W. B.; Trapp, B. D.; Yan, R. Bace1 modulates myelination in the central and peripheral nervous system. *Nat. Neurosci.* **2006**, *9*, 1520–1525.

(14) Cheret, C.; Willem, M.; Fricker, F. R.; Wende, H.; Wulf-Goldenberg, A.; Tahirovic, S.; Nave, K.-A.; Saftig, P.; Haass, C.; Garratt, A. N.; Bennett, D. L.; Birchmeier, C. Bace1 and Neuregulin-1 cooperate to control formation and maintenance of muscle spindles. *EMBO J.* **2013**, *32*, 2015–2028.

(15) McConlogue, L.; Buttini, M.; Anderson, J. P.; Brigham, E. F.; Chen, K. S.; Freedman, S. B.; Games, D.; Johnson-Wood, K.; Lee, M.; Zeller, M.; Liu, W.; Motter, R.; Sinha, S. Partial reduction of BACE1 has dramatic effects on Alzheimer plaque and synaptic pathology in APP transgenic mice. *J. Biol. Chem.* **2007**, *282*, 26326–26334.

(16) Wang, Y.-S.; Strickland, C.; Voigt, J. H.; Kennedy, M. E.; Beyer, B. M.; Senior, M. M.; Smith, E. M.; Nechuta, T. L.; Madison, V. S.; Czarniecki, M.; McKittrick, B. A.; Stamford, A. W.; Parker, E. M.; Hunter, J. C.; Greenlee, W. J.; Wyss, D. F. Application of fragment-based NMR screening, X-ray crystallography, structure-based design, and focused chemical library design to identify novel μM leads for the development of nM BACE-1 (β-site APP cleaving enzyme 1) inhibitors. *J. Med. Chem.* **2010**, *53*, 942–950.

(17) The CAS name represents the 3-aminothiadiazine tautomer, and the structures depicted in the manuscript represent the 3-iminothiadiazinane tautomer.

(18) Zhu, Z.; Sun, Z.-Y.; Ye, Y.; Voigt, J.; Strickland, C.; Smith, E. M.; Cumming, J.; Wang, L.; Wong, J.; Wang, Y.-S.; Wyss, D. F.; Chen, X.; Kuvelkar, R.; Kennedy, M. E.; Favreau, L.; Parker, E.; McKittrick, B. A.; Stamford, A.; Czarniecki, M.; Greenlee, W.; Hunter, J. C. Discovery of cyclic acylguanidines as highly potent and selective β-site amyloid cleaving enzyme (BACE) inhibitors: part I-inhibitor design and validation. *J. Med. Chem.* **2010**, *53*, 951–965.

(19) Stamford, A.; Strickland, C. Inhibitors of BACE for treating Alzheimer's disease: a fragment-based drug discovery story. *Curr. Opin. Chem. Biol.* **2013**, *17*, 320–328.

(20) Cumming, J. N.; Smith, E. M.; Wang, L.; Misiaszek, J.; Durkin, J.; Pan, J.; Iserloh, U.; Wu, Y.; Zhu, Z.; Strickland, C.; Voigt, J.; Chen, X.; Kennedy, M. E.; Kuvelkar, R.; Hyde, L. A.; Cox, K.; Favreau, L.; Czarniecki, M. F.; Greenlee, W. J.; McKittrick, B. A.; Parker, E. M.; Stamford, A. W. Structure based design of iminohydantoin BACE1 inhibitors: identification of an orally available, centrally active BACE1 inhibitor. *Bioorg. Med. Chem. Lett.* **2012**, *22*, 2444–2449.

(21) Stamford, A. W.; Scott, J. D.; Li, S. W.; Babu, S.; Tadesse, D.; Hunter, R.; Wu, Y.; Misiaszek, J.; Cumming, J. N.; Gilbert, E. J.; Huang, C.; McKittrick, B. A.; Hong, L.; Guo, T.; Zhu, Z.; Strickland, C.; Orth, P.; Voigt, J. H.; Kennedy, M. E.; Chen, X.; Kuvelkar, R.; Hodgson, R.; Hyde, L. A.; Cox, K.; Favreau, L.; Parker, E. M.; Greenlee, W. J. Discovery of an orally available, brain penetrant BACE1 inhibitor that affords robust CNS Aβ reduction. *ACS Med. Chem. Lett.* **2012**, *3*, 897–902.

(22) (a) Mandal, M.; Zhu, Z.; Cumming, J. N.; Liu, X.; Strickland, C.; Mazzola, R. D.; Caldwell, J. P.; Leach, P.; Grzelak, M.; Hyde, L.; Zhang, Q.; Terracina, G.; Zhang, L.; Chen, X.; Kuvelkar, R.; Kennedy, M. E.; Favreau, L.; Cox, K.; Orth, P.; Buevich, A.; Voigt, J.; Wang, H.; Kazakevich, I.; McKittrick, B. A.; Greenlee, W.; Parker, E. M.; Stamford, A. W. Design and validation of bicyclic iminopyrimidinones as beta amyloid cleaving enzyme-1 (BACE1) inhibitors: conformational constraint to favor a bioactive conformation. *J. Med. Chem.* **2012**, *55*, 9331–9345. (b) Mandal, M.; Wu, Y.; Misiaszek, J.; Li, G.; Buevich, A.; Caldwell, J. P.; Liu, X.; Mazzola, R. D.; Orth, P.; Strickland, C.; Voigt, J.; Wang, H.; Zhu, Z.; Chen, X.; Grzelak, M.; Hyde, L. A.; Kuvelkar, R.; Leach, P. T.; Terracina, G.; Zhang, L.; Zhang, Q.; Michener, M. S.; Smith, B.; Cox, K.; Grotz, D.; Favreau, L.; Mitra, K.; Kazakevich, I.; McKittrick, B. A.; Greenlee, W.; Kennedy, M. E.; Parker, E. M.; Cumming, J. N.; Stamford, A. W. Structure-based design of an iminoheterocyclic β-site amyloid precursor protein cleaving enzyme (BACE) inhibitor that lowers central Aβ in nonhuman primates. *J. Med. Chem.* **2016**, *59*, 3231–3248.

(23) (a) Zhu, Z.; McKittrick, B.; Sun, Z.-Y.; Ye, Y. C.; Voigt, J. H.; Strickland, C.; Smith, E. M.; Stamford, A.; Greenlee, W. J.; Wu, Y.; Iserloh, U.; Mazzola, R.; Caldwell, J.; Cumming, J.; Wang, L.; Guo, T.; Le, T. X. H.; Saionz, K. W.; Babu, S. D.; Hunter, R. C. Preparation of heterocyclic aspartyl protease inhibitors for treating various diseases. WO2005058311A1, 2005. (b) Malamas, M. S.; Erdei, J. J.; Gunawan, I. S.; Zhou, P.; Yan, Y.; Quagliato, D. A. Preparation of amino-5,5-diphenylimidazolone derivatives for inhibition of beta-secretase and treatment of β-amyloid-related diseases. US20050282825A1, 2005. (c) Albert, J. S.; Andisik, D.; Arnold, J.; Brown, D.; Callaghan, O.; Campbell, J.; Carr, R. A. E.; Chessari, G.; Congreve, M. S.; Edwards, P.; Empfield, J. R.; Frederickson, M.; Koether, G. M.; Krumrine, J.; Mauger, R.; Murray, C. W.; Patel, S.; Sylvester, M.; Throner, S. Preparation of substituted 2-aminopyrimidin-4-ones for treating or preventing Aβ-related pathologies. WO2006041404A1, 2006.

(24) Although we recognized the importance of pK_a to inhibitor properties, we were unable to make reliable pK_a predictions of the iminothiadiazinane class of inhibitors using standard ab initio quantum mechanical calculations performed by commercially available software packages.

(25) Ginman, T.; Viklund, J.; Malmström, J.; Blid, J.; Emond, R.; Forsblom, R.; Johansson, A.; Kers, A.; Lake, F.; Sehgelmeble, F.; Sterky, K. J.; Bergh, M.; Lindgren, A.; Johansson, P.; Jeppsson, F.; Fälting, J.; Gravenfors, Y.; Rahm, F. Core refinement toward permeable β-secretase (BACE-1) inhibitors with low hERG activity. *J. Med. Chem.* **2013**, *56*, 4181–4205.

(26) The PSA value was calculated using the method described in Ertl, P.; Rohde, B.; Selzer, P. Fast calculation of molecular polar surface area as a sum of fragment-based contributions and its application to the prediction of drug transport properties. *J. Med. Chem.* **2000**, *43*, 3714–3717 excluding the contribution from the sulfur atom.

(27) Scott, J. D.; Stamford, A. W.; Gilbert, E. J.; Cumming, J. N.; Iserloh, U.; Misiaszek, J. A.; Li, G. Iminothiadiazine dioxide compounds as BACE inhibitors and their preparation, compositions and use in the treatment of pathologies associated with beta-amyloid protein. WO2011044181A1, 2011.

(28) (a) Koike, M.; Nakanishi, H.; Saftig, P.; Ezaki, J.; Isahara, K.; Ohsawa, Y.; Schulz-Schaeffer, W.; Watanabe, T.; Waguri, S.; Kametaka, S.; Shibata, M.; Yamamoto, K.; Kominami, E.; Peters, C.; von Figura, K.; Uchiyama, Y. Cathepsin D deficiency induces lysosomal storage with ceroid lipofuscin in mouse CNS neurons. *J. Neurosci.* **2000**, *20*, 6898–6906. (b) Siintola, E.; Partanen, S.; Strömme, P.; Haapanen, A.; Haltia, M.; Maehlen, J.; Lehesjoki, A.-E.; Tyynelä, J. Cathepsin D deficiency underlies congenital human neuronal ceroid-lipofuscinosis. *Brain* **2006**, *129*, 1438–1445.

(29) May, P. C.; Dean, R. A.; Lowe, S. L.; Martenyi, F.; Sheehan, S. M.; Boggs, L. N.; Monk, S. A.; Mathes, B. M.; Mergott, D. J.; Watson, B. M.; Stout, S. L.; Timm, D. E.; LaBell, E. S.; Gonzales, C. R.; Nakano, M.; Jhee, S. S.; Yen, M.; Ereshefsky, L.; Lindstrom, T. D.; Calligaro, D. O.; Cocke, P. J.; Hall, D. G.; Friedrich, S.; Citron, M.; Audia, J. E. Robust central reduction of amyloid-β in humans with an orally available, non-peptidic β-secretase inhibitor. *J. Neurosci.* **2011**, *31*, 16507–16516.

(30) Fielden, M. R.; Werner, J.; Jamison, J. A.; Coppi, A.; Hickman, D.; Dunn, R. T., II; Trueblood, E.; Zhou, L.; Afshari, C. A.; Lightfoot-Dunn, R. Retinal toxicity induced by a novel β-secretase inhibitor in the Sprague-Dawley rat. *Toxicol. Pathol.* **2015**, *43*, 581–592.

(31) Independent of our work, selectivity of LY2811376 for BACE1 versus CatD was recently reported to be 6-fold. Butler, C. R; Brodney, M. A.; Beck, E. M.; Barreiro, G.; Nolan, C. E.; Pan, F.; Vajdos, F.; Parris, K.; Varghese, A. H.; Helal, C. J.; Lira, R.; Doran, S. D.; Riddell, D. R.; Buzon, L. M.; Dutra, J. K.; Martinez-Alsina, L. A.; Ogilvie, K.; Murray, J. C.; Young, J. M.; Atchison, K.; Robshaw, A.; Gonzales, C.;

Wang, J.; Zhang, Y.; O'Neill, B. T. Discovery of a series of efficient, centrally efficacious BACE1 inhibitors through structure-based drug design. *J. Med. Chem.* **2015**, *58*, 2678–2702.

(32) Zhu, Z.; McKittrick, B. A.; Sun, Z.-Y.; Ye, Y. C.; Voigt, J. H.; Strickland, C.; Smith, E. M.; Stamford, A.; Greenlee, W. J.; Mazzola, R.; Caldwell, J.; Cumming, J. N.; Wang, L.; Wu, Y.; Iserloh, U.; Guo, T.; Le, T. X. H.; Saionz, K. W.; Babu, S. D.; Hunter, R. C.; Morris, M. L.; Gu, H.; Qian, G.; Tadesse, D. Heterocyclic aspartyl protease inhibitors. US 20060111370, May 25, 2006.

(33) Baldwin, E. T.; Bhat, T. N.; Gulnik, S.; Hosur, M. V.; Sowder, R. C., II; Cachau, R. E.; Collins, J.; Silva, A. M.; Erickson, J. W. Crystal structures of native and inhibited forms of human cathepsin D: implications for lysosomal targeting and drug design. *Proc. Natl. Acad. Sci. U. S. A.* **1993**, *90*, 6796–6800.

(34) Rueeger, H.; Lueoend, R.; Rogel, O.; Rondeau, J.-M.; Möbitz, H.; Machauer, R.; Jacobson, L.; Staufenbiel, M.; Desrayaud, S.; Neumann, U. Discovery of cyclic sulfone hydroxyethylamines as potent and selective β-site APP-cleaving enzyme 1 (BACE1) inhibitors: structure-based design and in vivo reduction of amyloid β-peptides. *J. Med. Chem.* **2012**, *55*, 3364–3386.

(35) (a) Cox, C. D.; Breslin, M. J.; Whitman, D. B.; Coleman, P. J.; Garbaccio, R. M.; Fraley, M. E.; Zrada, M. M.; Buser, C. A.; Walsh, E. S.; Hamilton, K.; Lobell, R. B.; Tao, W.; Abrams, M. T.; South, V. J.; Huber, H. E.; Kohl, N. E.; Hartman, G. D. Kinesin spindle protein (KSP) inhibitors. Part V: discovery of 2-propylamino-2,4-diaryl-2,5-dihydropyrroles as potent, water-soluble KSP inhibitors, and modulation of their basicity by β-fluorination to overcome cellular efflux by P-glycoprotein. *Bioorg. Med. Chem. Lett.* **2007**, *17*, 2697–2702. (b) McDonald, I. M.; Mate, R. A.; Zusi, F. C.; Huang, H.; Post-Munson, D. J.; Ferrante, M. A.; Gallagher, L.; Bertekap, R. L., Jr.; Knox, R. J.; Robertson, B. J.; Harden, D. G.; Morgan, D. G.; Lodge, N. J.; Dworetzky, S. I.; Olson, R. E.; Macor, J. E. Discovery of a novel series of quinolone α7 nicotinic acetylcholine receptor agonists. *Bioorg. Med. Chem. Lett.* **2013**, *23*, 1684–1688. (c) Lerchner, A.; Machauer, R.; Betschart, C.; Veenstra, S.; Rueeger, H.; McCarthy, C.; Tintelnot-Blomley, M.; Jaton, A.-L.; Rabe, S.; Desrayaud, S.; Enz, A.; Staufenbiel, M.; Paganetti, P.; Rondeau, J.-M.; Neumann, U. Macrocyclic BACE-1 inhibitors acutely reduce Aβ in brain after po application. *Bioorg. Med. Chem. Lett.* **2010**, *20*, 603–607.

(36) (a) Hyde, L.; Chen, X.; Stahl, L.; Sondey, M.; Scott, J.; Cumming, J.; Stamford, A.; Parker, E.; Kennedy, M. Chronic BACE inhibition dramatically slows the rate of Aβ accumulation and the development of amyloid plaques in young TgCRND8 mice. *Alzheimer's Dementia* **2012**, *8*, P188. (b) Hyde, L.; Cantu, C.; Werner, B.; Chen, X.; Sondey, M.; Chen, M.; Weig, B.; LaShomb, A.; Lu, S.; Hodgson, R.; Scott, J.; Cumming, J.; Stamford, A.; Parker, E.; Kennedy, M. Chronic BACE inhibition halts further age-related increases in brain Aβ and amyloid plaques in aged TgCRND8 mice with established plaques. *Alzheimer's Dementia* **2012**, *8*, P188.

(37) Schärfer, C.; Schulz-Gasch, T.; Ehrlich, H.-C.; Guba, W.; Rarey, M.; Stahl, M. Torsion angle preferences in druglike chemical space: a comprehensive guide. *J. Med. Chem.* **2013**, *56*, 2016–2028.

(38) Kennedy, M. E.; Stamford, A. W.; Chen, X.; Cox, K.; Cumming, J. N.; Dockendorf, M. F.; Egan, M.; Ereshefsky, L.; Hodgson, R. A.; Hyde, L. A.; Jhee, S.; Kleijn, H. J.; Kuvelkar, R.; Li, W.; Mattson, B. A.; Mei, H.; Palcza, J.; Scott, J. D.; Tanen, M.; Troyer, M. D.; Tseng, J. L.; Stone, J. A.; Parker, E. M.; Forman, M. S. The BACE1 inhibitor verubecestat (MK-8931) reduces CNS β-amyloid in animal models and in Alzheimer's disease patients. *Sci. Transl. Med.* **2016**, *8*, 363ra150.

(39) Ostermann, N.; Eder, J.; Eidhoff, U.; Zink, F.; Hassiepen, U.; Worpenberg, S.; Maibaum, J.; Simic, O.; Hommel, U.; Gerhartz, B. Crystal structure of human BACE2 in complex with a hydroxyethyl-amine transition-state inhibitor. *J. Mol. Biol.* **2006**, *355*, 249–261.

(40) (a) Kelder, J.; Grootenhuis, P. D. J.; Bayada, D. M.; Delbressine, L. P. C.; Ploemen, J.-P. Polar molecular surface as a dominating determinant for oral absorption and brain penetration of drugs. *Pharm. Res.* **1999**, *16*, 1514–1519. (b) Van de Waterbeemd, H.; Camenisch, G.; Folkers, G.; Chretien, J. R.; Raevsky, O. A. Estimation of blood–

brain barrier crossing of drugs using molecular size and shape, and H-bonding descriptors. *J. Drug Targeting* **1998**, *6*, 151–165.

(41) Alex, A.; Millan, D. S.; Perez, M.; Wakenhut, F.; Whitlock, G. A. Intramolecular hydrogen bonding to improve membrane permeability and absorption in beyond rule of five chemical space. *MedChemComm* **2011**, *2*, 669–674.

(42) Tang, H.; Mayersohn, M. A novel model for prediction of human drug clearance by allometric scaling. *Drug Metab. Dispos.* **2005**, *33*, 1297–1303 For **3**, the exponent b was set to 0.75 for all three species used to calculate the projected human dose.

(43) Diller, J. D. In silico hERG modelling: challenges and progress. *Curr. Comput.-Aided Drug Des.* **2009**, *5*, 106–121.

(44) Roden, D. M. Drug-induced prolongation of the QT interval. *N. Engl. J. Med.* **2004**, *350*, 1013–1022.

(45) (a) Rochin, L.; Hurbain, I.; Serneels, L.; Fort, C.; Watt, B.; Leblanc, P.; Marks, M. S.; De Strooper, B.; Raposo, G.; van Niel, G. BACE2 processes PMEL to form the melanosome amyloid matrix in pigment cells. *Proc. Natl. Acad. Sci. U. S. A.* **2013**, *110*, 10658–10663. (b) Shimshek, D. R.; Jacobson, L. H.; Kolly, C.; Zamurovic, N.; Balavenkatraman, K. K.; Morawiec, L.; Kreutzer, R.; Schelle, J.; Jucker, M.; Bertschi, B.; Theil, D.; Heier, A.; Bigot, K.; Beltz, K.; Machauer, R.; Brzak, I.; Perrot, L.; Neumann, U. Pharmacological BACE1 and BACE2 inhibition induces hair depigmentation by inhibiting PMEL17 processing in mice. *Sci. Rep.* **2016**, *6*, 21917.

(46) Esterházy, D.; Stützer, I.; Wang, H.; Rechsteiner, M. P.; Beauchamp, J.; Döbeli, H.; Hilpert, H.; Matile, H.; Prummer, M.; Schmidt, A.; Lieske, N.; Boehm, B.; Marselli, L.; Bosco, D.; Kerr-Conte, J.; Aebersold, R.; Spinas, G. A.; Moch, H.; Migliorini, C.; Stoffel, M. BACE2 is a β cell-enriched protease that regulates pancreatic β cell function and mass. *Cell Metab.* **2011**, *14*, 365–377.

(47) Velázquez, F.; Arasappan, A.; Chen, K.; Sannigrahi, M.; Venkatraman, S.; McPhail, A. T.; Chan, T.-M.; Shih, N.-Y.; Njoroge, F. G. Stereoselective synthesis of β-substituted β-amino sulfones and sulfonamides via addition of sulfonyl anions to chiral N-sulfinyl imines. *Org. Lett.* **2006**, *8*, 789–792.

(48) Brak, K.; Barrett, K. T.; Ellman, J. A. General one-pot method for the preparation of N-tert-butanesulfinylamine diastereomer mixtures as standards for stereoselectivity determinations. *J. Org. Chem.* **2009**, *74*, 3606–3608.

(49) Huang, B.-S.; Chello, P. L.; Yip, L.; Parham, J. C. Synthesis and properties of the sulfonyl analogues of 4(5)-aminoimidazole-5(4)-carboxamide, 4(5)-(formylamino)imidazole-5(4)-carboxamide, guanine, and xanthine. *J. Med. Chem.* **1980**, *23*, 575–577.

(50) A manufacturing route to verubecestat is described in Thaisrivongs, D. A.; Miller, S. P.; Molinaro, C.; Chen, Q.; Song, Z. J.; Tan, L.; Chen, L.; Wenyong Chen, W.; Lekhal, A.; Pulicare, S. K.; Xu, Y. Synthesis of verubecestat (MK-8931), a BACE1 inhibitor for the treatment of Alzheimer's disease. *Org. Lett.* **2016**, DOI: 10.1021/acs.orglett.6b01793.